

c. Variation of SAR along the y-axis parallel to the narrower dimension of the waveguide at height $z = 4$ mm.
Fig. 4. Comparison of the measured and calculated SAR variations for a planar phantom of base thickness 2.0 mm and internal dimensions $30.5 \times 41.9 \times 20$ cm for a WR 187 open-ended waveguide radiator placed 10 mm below the bottommost surface of the lossy tissue-simulant phantom. Frequency = 5.8 GHz.

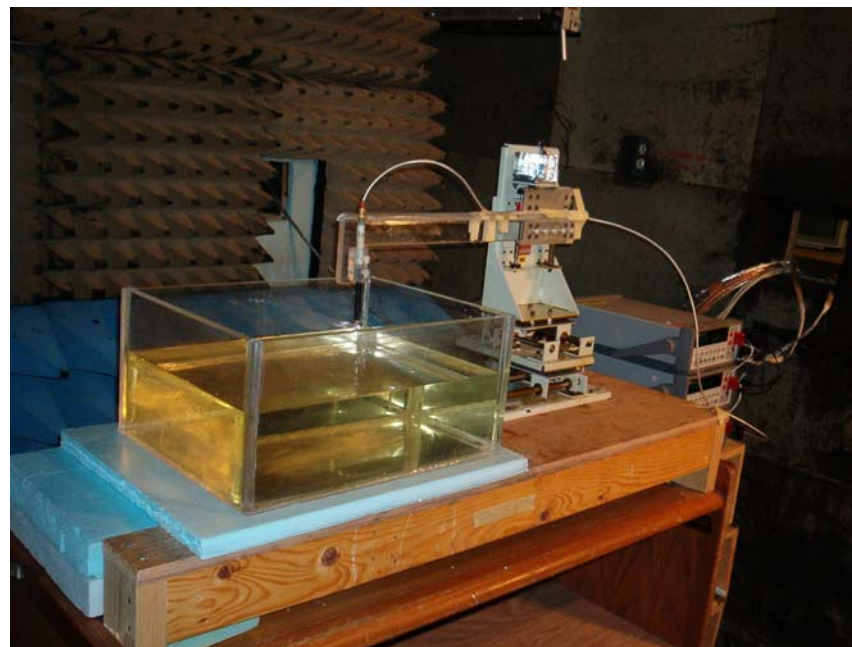


Fig. 5. Photograph of the planar model with the 3-D stepper motor system used for measurement of SAR variation for comparison with FDTD calculations.

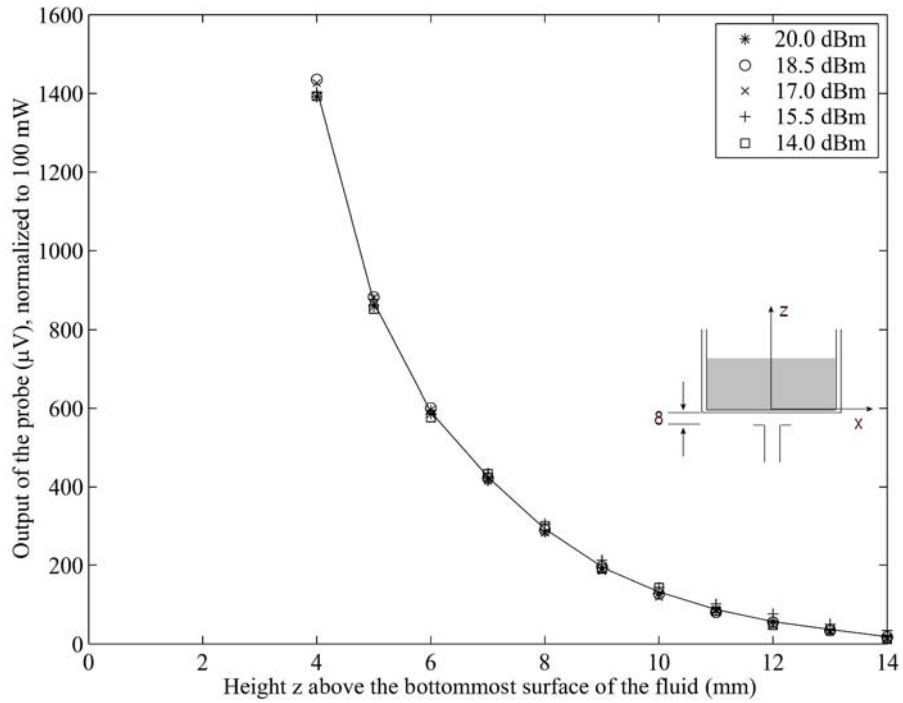
A triaxial Narda Model 8021 E-field probe is used to determine the internal electric fields. The positioning repeatability of the stepper motor system moving the E-field probe is within ± 0.1 mm. Outputs from the three channels of the E-field probe are dc voltages, the sum of which is proportional to the square of the internal electric fields ($|E_i|^2$) from which the SAR can be obtained from the equation: $SAR = \sigma(|E_i|^2)/\rho$, where σ and ρ are the conductivity and mass density of the tissue-simulant material, respectively [13]. The dc voltages for the three channels of the E-field probe are read by three HP 34401A multimeters and sent to the computer via an HPIB interface. The setup is carefully grounded and shielded to reduce the noise due to the electromagnetic interference (EMI).

B. E-Field Probe

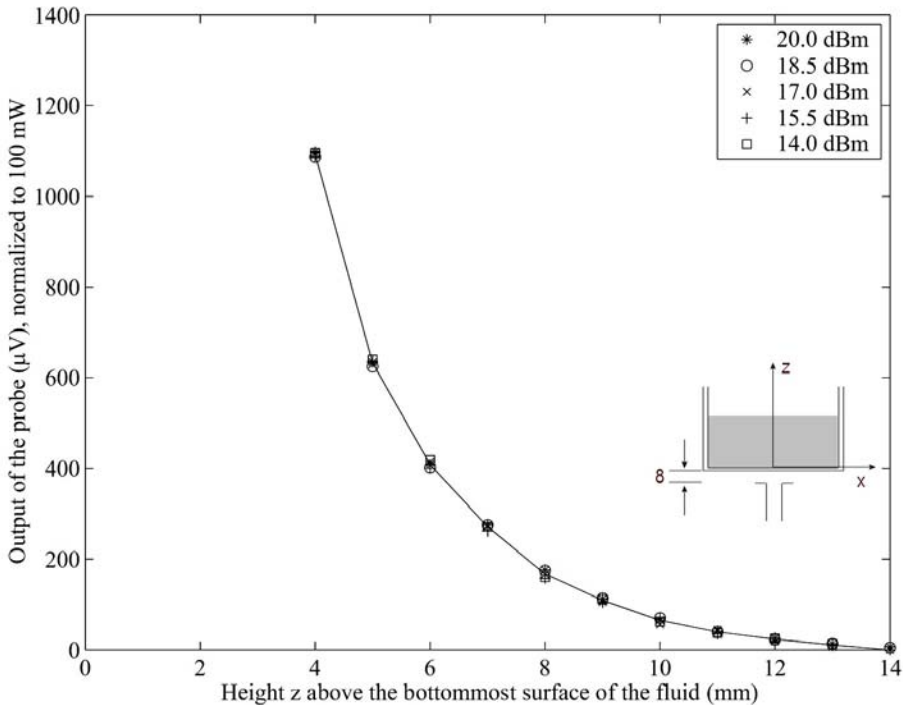
The nonperturbing implantable E-field probe used in the setup was originally developed by Bassen et al. [14] and is manufactured by L3/Narda Microwave Corporation, Hauppauge, NY as Model 8021 E-field probe. In the probe, three orthogonal miniature dipoles each of length approximately 2.5 mm are placed on a triangular-beam substrate. Each dipole is loaded with a small Schottky diode and connected to the external circuitry by high resistance ($2 M\Omega \pm 40\%$) leads to reduce secondary pickups. The entire structure is then encapsulated with a low dielectric constant insulating material. The probe thus constructed has a very small diameter (4 mm), which results in a relatively small perturbation of the internal electric field. The probe is rated for frequencies up to 3 GHz for tissue-simulant media, but is presently used for system validation at frequencies in the 5 to 6 GHz range. Consequently, the probe had to be checked for square-law performance, and isotropy for use at these higher frequencies.

- 1. Test for Square-Law Region:** It is necessary to operate the E-field probe in the square-law region for each of the diodes so that the sum of the dc voltage outputs from the three dipoles is proportional to the square of the internal electric field ($|E_i|^2$). Fortunately, the personal wireless devices such as the PCs induce SARs that are generally less than 5-6 W/kg even for closest locations to the body. For SAR measurements, it is, therefore, necessary that the E-field probe be checked for square-law behavior for SARs up to such values that are likely to be encountered. Such a test may be conducted using a canonical lossy body such as a rectangular box used here. By varying the radiated power of the waveguide, the output of the probe should increase linearly with the applied power for each of the test locations.

Shown in Fig. 6a and b are the results of the tests performed to check the square-law behavior of the E-field probe used in our setup at 5.25 and 5.8 GHz, respectively. Used as the radiator is the WR 187 waveguide placed at a distance of 8 mm below the base of the planar phantom (10 mm below the bottom surface of the tissue-simulant fluid as recommended in [6]).



a. Test for square-law behavior at 5.25 GHz.



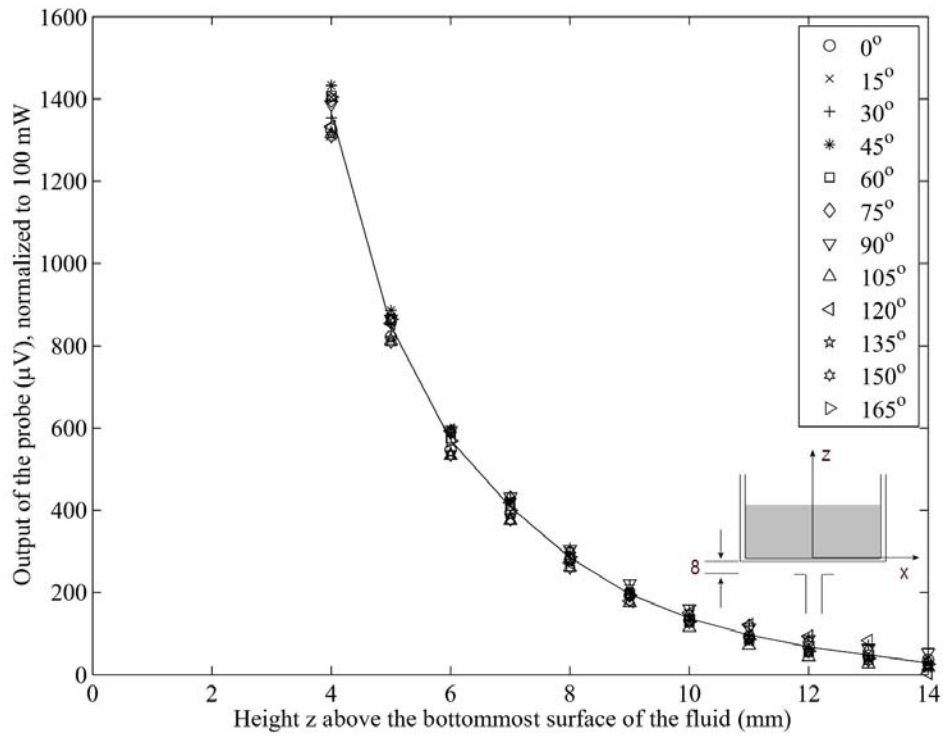
b. Test for square-law behavior at 5.8 GHz.

Fig. 6. Variation of the output voltage (proportional to $|E_i|^2$) for different radiated powers normalized to 100 mW (20 dBm).

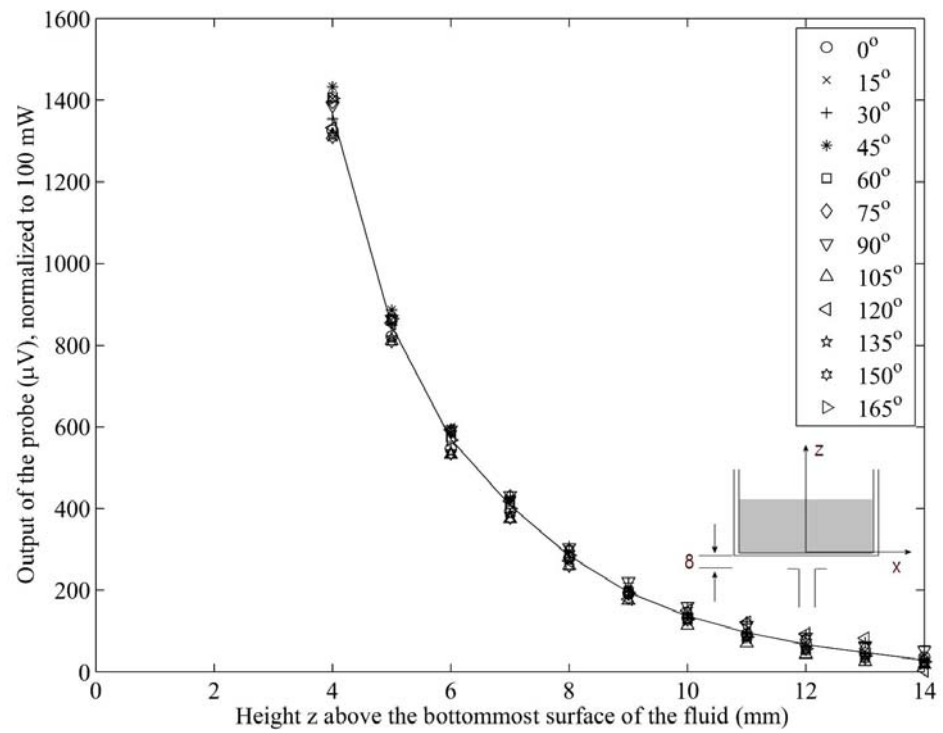
Since the dc voltage outputs of the probe are fairly similar when normalized to a radiated power of 100 mW, the square-law behavior is demonstrated and an output voltage that is proportional to $|E_i|^2$ is obtained within $\pm 2.2\%$ both at 5.25 and 5.8 GHz.

2. **Test for Isotropy of the Probe:** Another important characteristic of the probe that affects the measurement accuracy is its isotropy. Since the orientation of the induced electric field is generally unknown, the E-field probe should be relatively isotropic in its response to the orientation of the E-field. Shown in Fig. 7a and b are the test results of the E-field probe used in our setup at 5.25 and 5.8 GHz, respectively. The E-field probe was rotated around its axis from 0-180° in incremental steps of 15°. Because of the alternating nature of the fields, angles of θ and $180^\circ + \theta$ are identical, hence 0-165° rotation of the E-field probe was considered to be adequate to cover the entire 360° rotation of the probe. As seen in Fig. 7a and b, an isotropy of less than ± 0.18 dB ($\pm 4.3\%$) was observed for this E-field probe both at 5.25 and 5.8 GHz.
3. **Calibration of the E-Field Probe:** Since the voltage output of the E-field probe is proportional to the square of the internal electric field ($|E_i|^2$), the SAR is, therefore, proportional to the voltage output of the E-field probe by a proportionality constant C. The constant C is defined as the calibration factor and is frequency and material dependent. It is measured to calibrate the probe at the various frequencies of interest using the appropriate tissue-simulating materials for the respective frequencies.

Canonical geometries such as waveguides, rectangular slabs, and layered or homogeneous spheres have, in the past, been used for the calibration of the implantable E-field probe [15-17] albeit at lower frequencies. Since the FDTD method has been carefully validated to solve electromagnetic problems for a variety of near-field exposure geometries [18], we were able to calibrate the Narda E-field probe by comparing the measured variations of the probe voltage (proportional to $|E_i|^2$) against the FDTD-calculated variations of the SARs for the planar phantom of base thickness 2.0 mm ($\epsilon_r = 2.56$) and internal dimensions $30.5 \times 41.9 \times 20$ cm irradiated by the WR 187 waveguide placed below this phantom as previously described in Section. II. Shown in Figs. 6a, b and 7a, b are the comparisons between the experimentally measured and FDTD-calculated variations of the SAR distributions in the tissue-simulant fluid. Since there are excellent agreements between the calculated SARs and the measured variations of the voltage outputs of the E-field probe, it is possible to calculate the calibration factors at the respective frequencies by fitting the measured data to the FDTD-calculated results by means of the least mean-square error (LMSE) method. For the Narda Model 8021 E-field probe used in our setup, the calibration factor is determined to be 2.98 (mW/kg)/ μ V $\pm 5\%$ both at 5.25 and 5.8 GHz, respectively.



a. 5.25 GHz.



b. 5.8 GHz.

Fig. 7. Test for isotropy.

IV. Need for Extrapolation

Because of the physical separation of the three orthogonal pickup dipoles from the tip of the E-field probe, the SAR measurements cannot be taken any closer than about 3 mm from the bottom surface of the phantom fluid. As given in Figs. 8 and 9, we have measured the SARs with 2 mm resolution at heights of 4, 6, 8, 10, 12 and 14 mm above the bottom surface of the phantom fluid. We have tried second-, third-, fourth-, and fifth-order polynomial least-square fits to extrapolate the measured data to obtain SARs closer to the bottom of the lossy fluid. As seen in Figs. 8 and 9, the second- and third-order polynomials underestimate the SARs while the fifth-order polynomial overestimates the SAR distribution. An excellent least-square fit to the numerically-calculated SAR variations is obtained by using a fourth-order polynomial to extrapolate the measured data both at 5.25 and 5.8 GHz.

After identifying the region of the highest SAR, the SAR distributions were measured with a finer resolution of 2 mm in order to obtain the peak 1 cm^3 or 1-g SAR. Here too, the SAR measurements were performed for the xy planes at heights z of 4, 6, 8, 10, 12, and 14 mm from the bottom surface of the body-simulant fluid. The SARs thus measured were extrapolated using a fourth-order least-square fit to the measured data to obtain values at 1, 3, 5, 7, and 9 mm height and used to obtain peak 1-g SARs. For a radiated power of 100 mW, the SARs thus obtained with 2 mm resolution for xy planes at heights z of 1, 3, 5, 7, and 9 mm for the peak SAR region of volume $10 \times 10 \times 10$ mm were used to obtain peak 1-g SAR at 5.25 and 5.8 GHz, respectively. The experimentally-determined peak 1-g SARs for 100 mW of radiated power of 3.678 and 3.947 W/kg are extremely close to the FDTD-calculated 1-g SARs for this waveguide irradiator of 3.580 and 3.946 W/kg at 5.25 and 5.80 GHz, respectively.

V. Conclusions

We have developed an open-ended waveguide irradiation system for validation of the SAR measurement system and/or for E-field probe calibration in the 802.11a frequency band 5.15 to 5.825 GHz. A fourth-order polynomial least-square fit to the experimental data gives SAR variations close to the bottom surface of the phantom that are in excellent agreement with those obtained using the FDTD method. The experimentally-determined peak 1-g SARs are within 1 to 2 percent of those obtained using the FDTD numerical calculations.

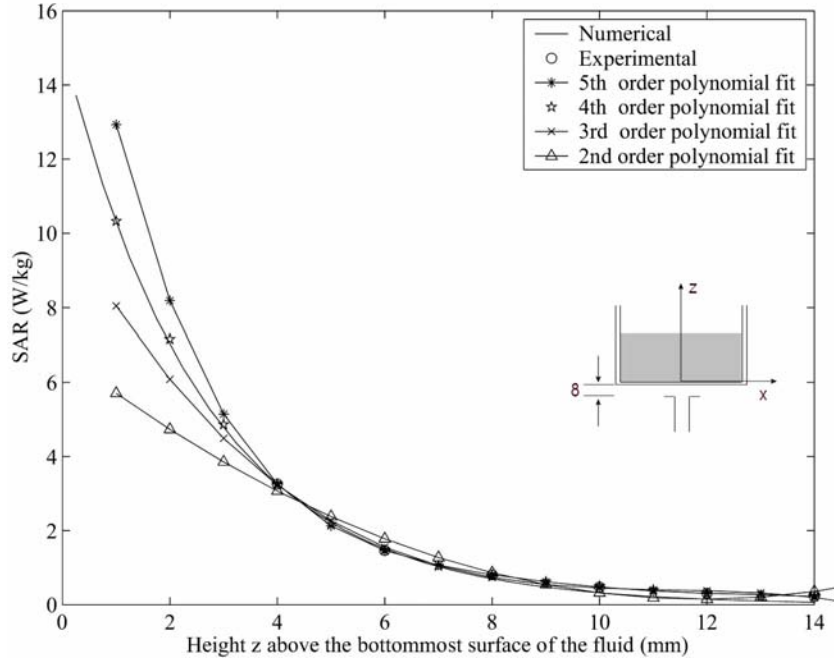


Fig. 8. Comparison of the experimentally measured and FDTD-calculated variation of the SAR with depth in the body-simulant planar phantom at 5.25 GHz. Also shown are the SARs extrapolated from experimental values to heights of 1, 3, 5, 7 and 9 mm above the bottom of the phantom using second-, third-, fourth-, and fifth-order least-square fit polynomials.

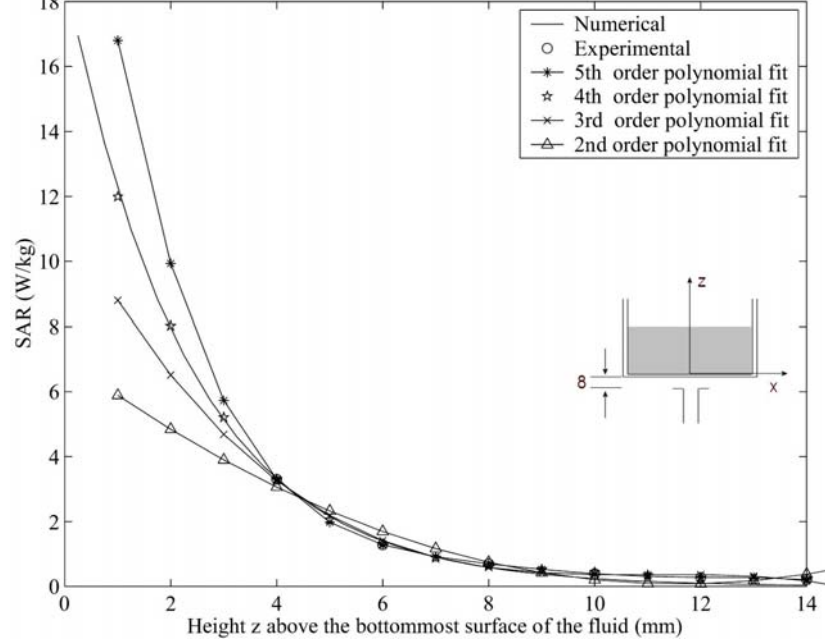


Fig. 9. Comparison of the experimentally measured and FDTD-calculated variation of the SAR with depth in the body-simulant planar phantom at 5.8 GHz. Also shown are the SARs extrapolated from experimental values to heights of 1, 3, 5, 7 and 9 mm above the bottom of the phantom using second-, third-, fourth-, and fifth-order least-square fit polynomials.

REFERENCES

1. IEEE Std. C95.1, "IEEE Standard for Safety Levels with Respect to Human Exposure to Radiofrequency Electromagnetic Fields, 3 kHz to 300 GHz," Institute of Electrical and Electronics Engineers, Piscataway, NJ, 1999.
2. ICNIRP (International Commission on Non-Ionizing Radiation Protection), "Guidelines for limiting exposure to time-varying electric, magnetic, and electromagnetic fields (up to 300 GHz)", *Health Physics*, Vol. 74, pp. 494-522, 1998.
3. IEEE Standards Coordinating Committee 34 Draft Standard, "Recommended Practice for Determining the Peak Spatial-Average Specific Absorption Rate (SAR) in the Human Body Due to Wireless Communications Devices: Experimental Techniques," Institute of Electrical and Electronics Engineers, 2002.
4. CENELEC EN50361, "Basic Standard for Measurement of Specific Absorption Rate Related to Human Exposure to Electromagnetic Fields from Mobile Telephones (300-MHz-3 GHz), CENELEC European Committee for Electrotechnical Standardization, rue de Stassart 35, B-1050, Brussels, Belgium.
5. IEC TC 106/PT62209, "Evaluation of Human Exposure to Radiofrequency Fields from Handheld and Body-Mounted Wireless Communications Devices in the Frequency Range of 30 MHz to 6 GHz: Human Models, Instrumentation Procedures," Draft Standard in preparation, 2003.
6. U.S. Federal Communications Commission (FCC), "Additional Information for Evaluating Compliance of Mobile and Portable Devices with FCC Limits for Human Exposure to Radiofrequency Emissions," Supplement C Edition 01-01 to OET Bulletin 65 Edition 97-01, June 2001.
7. A. Taflove (Ed.), *Advances in Computational Electrodynamics: The Finite-Difference Time-Domain Method*, Artech House, Boston, MA, 1998.
8. A. Taflove and S. C. Hagness, *Computational Electrodynamics: The Finite-Difference Time-Domain Method*, Artech House, Boston, MA, 2000.
9. P. J. Dimbylow and S. M. Mann, "SAR Calculations in an Anatomically-Based Realistic Model of the Head for Mobile Communication Transceivers at 900 MHz and 1.8 GHz," *Physics in Med. And Biol.*, Vol. 39, pp. 1537-1553, 1994.
10. O. P. Gandhi and J. Y. Chen, "Electromagnetic Absorption in the Human Head from Experimental 6 GHz Handheld Transceivers," *IEEE Trans. On Electromag. Compat.*, Vol. 37, pp. 547-558, 1995.

11. M. A. Jensen and Y. Rahmat-Samii, "EM Interaction in Handset Antennas and a Human in Personal Communications," *Proc. IEEE*, Vol. 83, pp. 7-17, 1995.
12. M. Okoniewski and M. A. Stuchly, "A Study of Handset Antenna and Human Body Interaction, *IEEE Trans. On Microwave Theory and Tech.*, Vol. 44, pp. 1855-1864, 1996.
13. M. A. Stuchly and S. S. Stuchly, "Experimental Radio and Microwave Dosimetry, " in *Handbook of Biological Effects of Electromagnetic Fields*, 2nd ed., C. Polk and E. Postow, Eds. Boca Raton, FL: CRC, pp. 295-336, 1996.
14. H. I. Bassen and G. S. Smith, "Electric Field Probes – a Review," *IEEE Trans. Antennas Propagat.*, Vol. AP-31, pp. 710-718, September 1983.
15. D. Hill, "Waveguide Techniques for the Calibration of Miniature Electric Field Probes for Use in Microwave Bioeffects Studies," *IEEE Trans. Microwave Theory Tech.*, Vol. MTT-30, pp. 92-94, 1982.
16. N. Kuster and Q. Balzano, "Energy Absorption Mechanism by Biological Bodies in the Near Field of Dipole Antennas Above 300 MHz," *IEEE Trans. Veh. Technol.*, Vol. 41, pp. 17-23, February 1992.
17. M. A. Stuchly, S. S. Stuchly, and A. Kraszewski, "Implantable Electric Field Probes – Some Performance Characteristics," *IEEE Trans. Biomed. Eng.*, Vol. BME-31, pp. 526-531, July 1984.
18. C. M. Furse, Q. S. Yu, and O. P. Gandhi, "Validation of the Finite-Difference Time-Domain Method for Near-Field Bioelectromagnetic Simulations," *Microwave and Optical Technology Letters*, Vol. 16, pp. 341-345, 1997.

APPENDIX E

Uncertainty Analysis

The uncertainty analysis of the University of Utah SAR Measurement System is given in Table E.1. Several of the numbers on tolerances are obtained by following procedures similar to those detailed in [3], while others have been obtained using methods suggested in [5].

Table E.1. Uncertainty analysis of the University of Utah SAR Measurement System.

Uncertainty Component	Uncertainty Value ± %	Probability Distribution	Divisor	C_i 1-g	Standard Unc. u_i ± %	v_i
Measurement System						
Probe calibration	2.0	N	1	1	2.0	∞
Axial isotropy of the probe	4.0	R	$\sqrt{3}$	$(1-c_p)^{1/2}$	1.6	∞
Hemispherical isotropy of the probe	5.5	R	$\sqrt{3}$	$\sqrt{c_p}$	0.0	∞
Boundary effect	0.8	R	$\sqrt{3}$	1	0.5	∞
Probe linearity	3.0	R	$\sqrt{3}$	1	1.7	∞
System detection limits	1.0	R	$\sqrt{3}$	1	0.6	∞
Readout electronics	1.0	N	1	1	1.0	∞
Response time	0.0	R	$\sqrt{3}$	1	0.0	∞
Integration time	0.5	R	$\sqrt{3}$	1	0.3	∞
RF ambient conditions	0	R	$\sqrt{3}$	1	0	∞
Probe positioner mechanical tolerance	0.5	R	$\sqrt{3}$	1	0.3	∞
Probe positioning with respect to phantom shell	2.0	R	$\sqrt{3}$	1	1.2	∞
Extrapolation, interpolation, & integration algorithms for maximum SAR evaluation	5.0	R	$\sqrt{3}$	1	2.9	∞
Test Sample Related						
Device positioning	3	R	$\sqrt{3}$	1	1.7	11
Device holder uncertainty	3	R	$\sqrt{3}$	1	1.7	7
Output power variation – SAR drift measurement	5	R	$\sqrt{3}$	1	2.9	∞
Phantom and Tissue Parameters						
Phantom uncertainty – base thickness tolerance	10.0	R	$\sqrt{3}$	1	5.8	∞
Liquid conductivity – deviation from target values	0.4	R	$\sqrt{3}$	0.7	0.2	∞
Liquid conductivity – measurement uncertainty	1.5	R	$\sqrt{3}$	0.7	0.6	∞
Liquid permittivity – deviation from target values	0.8	R	$\sqrt{3}$	0.6	0.3	∞
Liquid permittivity – measurement uncertainty	3.5	R	$\sqrt{3}$	0.6	1.2	∞
Combined Standard Uncertainty						
Expanded Uncertainty (95% Confidence Level)						
			RSS		8.3	
					± 16.6	

APPENDIX F

COARSE SCANS FOR THE HIGHEST SAR REGION FOR THE SENAO MODEL NL-5354 CB PLUS ARIES2 CARDBUS ADAPTER (FCC ID# NI3-AT53V214) WITH DELL MODEL PP01L HOST COMPUTER

January 29, 2004

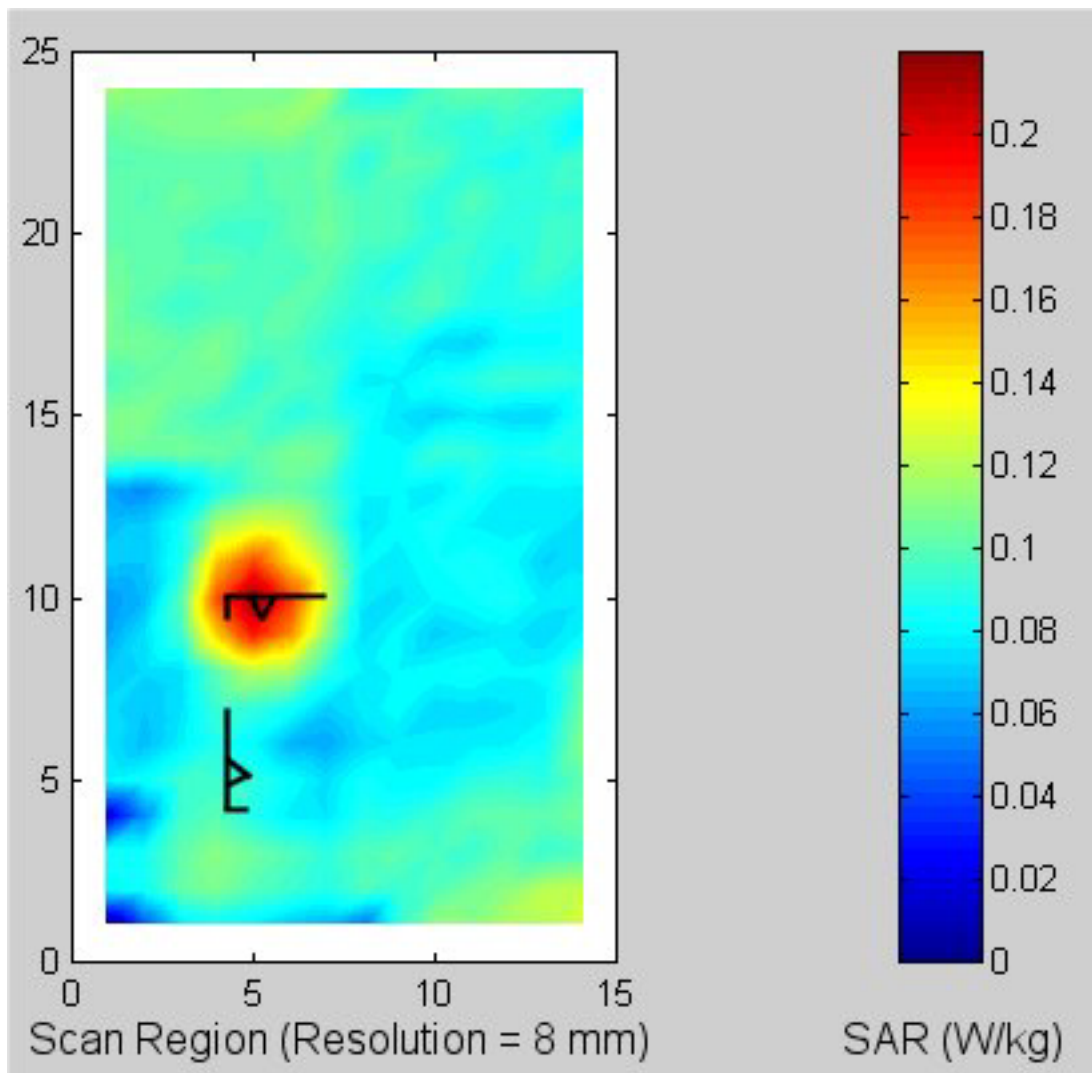


Fig. F.1. **Above-lap position (Configuration 1).** Normal mode at 5.26 GHz. Coarse scan for the highest SAR region for the Senao Model NL-5354 CB Plus Aries2 Cardbus Adapter inserted into Dell Model PP01L Host Computer.

Table F.1. **Above-lap position (Configuration 1). Normal mode at 5.26 GHz.** The SARs measured for the Senao Model NL-5354 CB Plus Aries2 Cardbus Adapter (FCC ID# NI3-AT53V214) inserted into Dell Model PP01L Host Computer.

1-g SAR = 0.237 W/kg

January 29, 2004

a. At depth of 1 mm

0.496	0.573	0.553	0.492	0.486
0.503	0.538	0.560	0.539	0.567
0.565	0.571	0.612	0.557	0.493
0.490	0.475	0.596	0.570	0.559
0.404	0.547	0.563	0.502	0.451

b. At depth of 3 mm

0.272	0.295	0.297	0.288	0.283
0.275	0.293	0.297	0.302	0.307
0.285	0.291	0.302	0.289	0.279
0.253	0.265	0.288	0.295	0.286
0.238	0.274	0.282	0.277	0.268

c. At depth of 5 mm

0.161	0.168	0.173	0.171	0.174
0.160	0.171	0.167	0.178	0.179
0.155	0.160	0.160	0.159	0.166
0.140	0.155	0.157	0.167	0.163
0.153	0.154	0.155	0.166	0.170

d. At depth of 7 mm

0.116	0.121	0.122	0.114	0.120
0.110	0.118	0.113	0.123	0.126
0.106	0.108	0.108	0.107	0.113
0.097	0.107	0.115	0.116	0.116
0.114	0.112	0.110	0.120	0.123

e. At depth of 9 mm

0.098	0.105	0.103	0.091	0.096
0.089	0.095	0.094	0.102	0.105
0.092	0.089	0.091	0.090	0.091
0.083	0.089	0.101	0.095	0.098
0.095	0.097	0.099	0.102	0.102

January 29, 2004

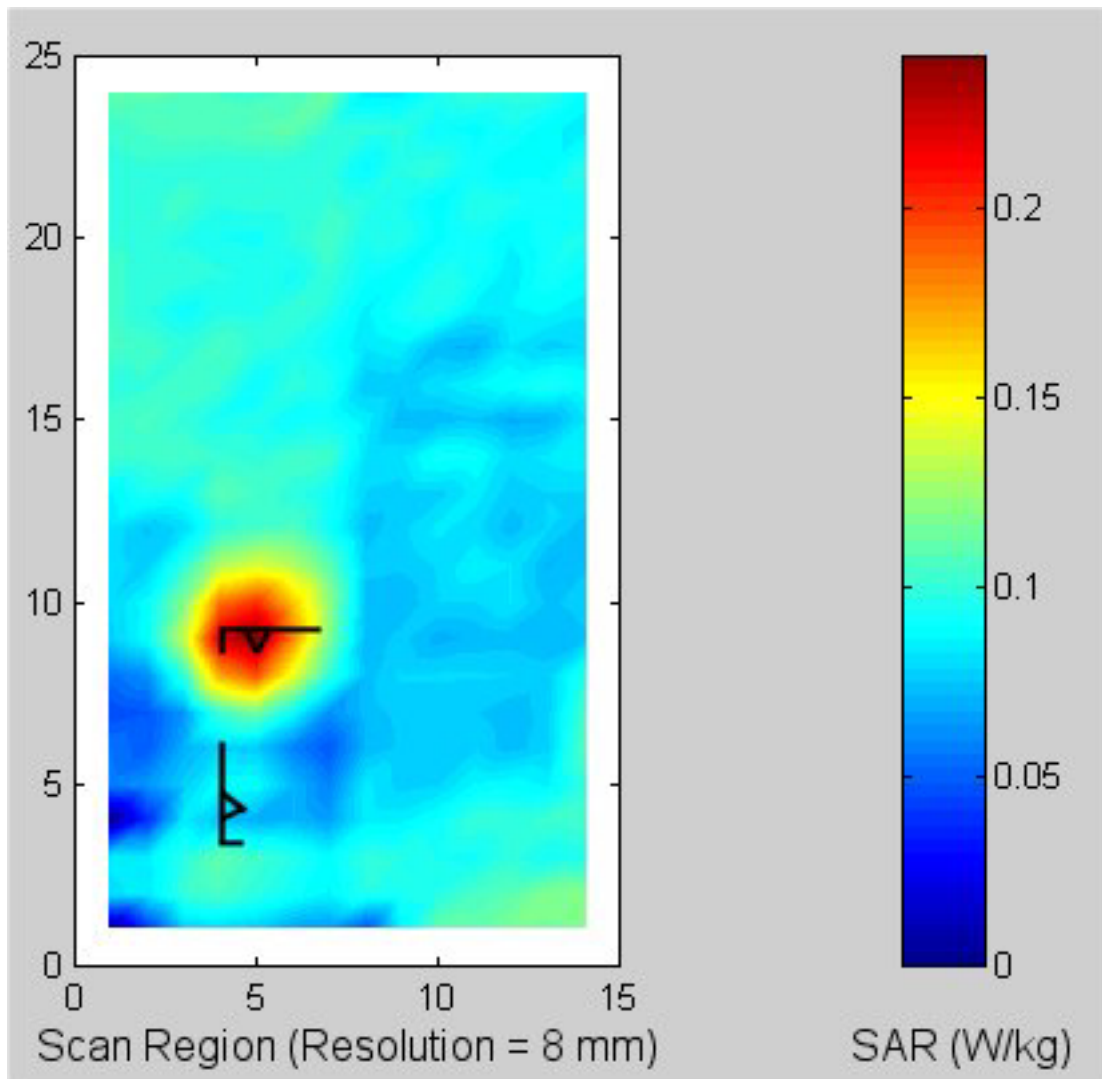


Fig. F.2. **Above-lap position (Configuration 1).** Normal mode at 5.32 GHz. Coarse scan for the highest SAR region for the Senao Model NL-5354 CB Plus Aries2 Wireless Cardbus Adapter inserted into Dell Model PP01L Host Computer.

Table F.2. **Above-lap position (Configuration 1). Normal mode at 5.32 GHz.** The SARs measured for the Senao Model NL-5354 CB Plus Aries2 Cardbus Adapter (FCC ID# NI3-AT53V214) inserted into Dell Model PP01L Host Computer.

1-g SAR = 0.263 W/kg

January 29, 2004

a. At depth of 1 mm

0.593	0.556	0.622	0.665	0.541
0.511	0.645	0.656	0.633	0.555
0.575	0.632	0.736	0.651	0.598
0.620	0.673	0.623	0.598	0.572
0.602	0.587	0.700	0.628	0.671

b. At depth of 3 mm

0.293	0.298	0.320	0.320	0.290
0.286	0.322	0.327	0.315	0.307
0.309	0.309	0.339	0.331	0.321
0.317	0.333	0.331	0.322	0.308
0.296	0.309	0.337	0.325	0.323

c. At depth of 5 mm

0.161	0.172	0.177	0.168	0.164
0.166	0.170	0.174	0.168	0.178
0.173	0.160	0.166	0.181	0.178
0.174	0.178	0.185	0.180	0.171
0.156	0.170	0.173	0.180	0.170

d. At depth of 7 mm

0.116	0.119	0.122	0.114	0.108
0.110	0.112	0.115	0.114	0.120
0.113	0.105	0.109	0.123	0.115
0.119	0.120	0.124	0.117	0.110
0.103	0.111	0.113	0.123	0.118

e. At depth of 9 mm

0.102	0.100	0.105	0.096	0.085
0.089	0.092	0.096	0.096	0.095
0.088	0.087	0.094	0.102	0.091
0.102	0.101	0.100	0.093	0.087
0.084	0.088	0.095	0.103	0.100

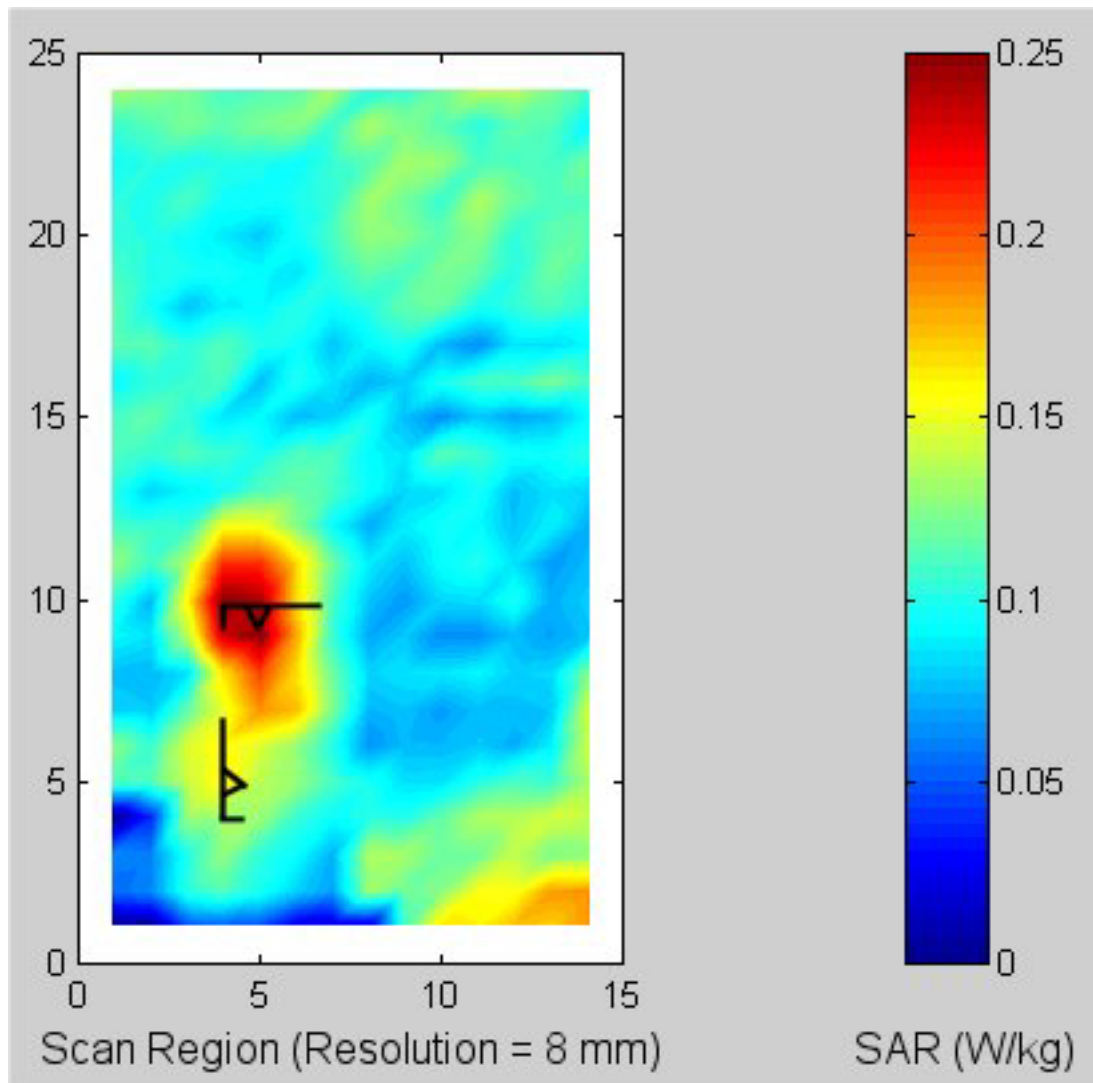


Fig. F.3. **Above-lap position (Configuration 1). Normal mode at 5.805 GHz.** Coarse scan for the highest SAR region for the Senao Model NL-5354 CB Plus Aries2 Wireless Cardbus Adapter inserted into Dell Model PP01L Host Computer.

Table F.3. **Above-lap position (Configuration 1). Normal mode at 5.805 GHz.** The SARs measured for the Senao Model NL-5354 CB Plus Aries2 Cardbus Adapter (FCC ID# NI3-AT53V214) inserted into Dell Model PP01L Host Computer.

1-g SAR = 0.253 W/kg

January 29, 2004

a. At depth of 1 mm

0.592	0.587	0.594	0.646	0.570
0.556	0.589	0.621	0.618	0.635
0.522	0.565	0.713	0.580	0.476
0.478	0.507	0.566	0.418	0.506
0.536	0.502	0.522	0.458	0.421

b. At depth of 3 mm

0.297	0.304	0.307	0.314	0.302
0.296	0.310	0.321	0.322	0.321
0.301	0.293	0.337	0.303	0.276
0.260	0.280	0.294	0.256	0.276
0.276	0.288	0.296	0.270	0.268

c. At depth of 5 mm

0.171	0.172	0.174	0.168	0.172
0.174	0.183	0.185	0.183	0.179
0.179	0.172	0.178	0.170	0.171
0.164	0.169	0.171	0.165	0.166
0.162	0.185	0.191	0.180	0.180

d. At depth of 7 mm

0.129	0.123	0.123	0.119	0.121
0.128	0.136	0.135	0.129	0.128
0.121	0.129	0.127	0.120	0.125
0.129	0.123	0.127	0.122	0.123
0.125	0.144	0.149	0.143	0.137

e. At depth of 9 mm

0.115	0.110	0.107	0.106	0.106
0.114	0.118	0.117	0.112	0.113
0.100	0.114	0.113	0.108	0.111
0.116	0.106	0.114	0.109	0.110
0.117	0.130	0.131	0.129	0.118

January 29, 2004

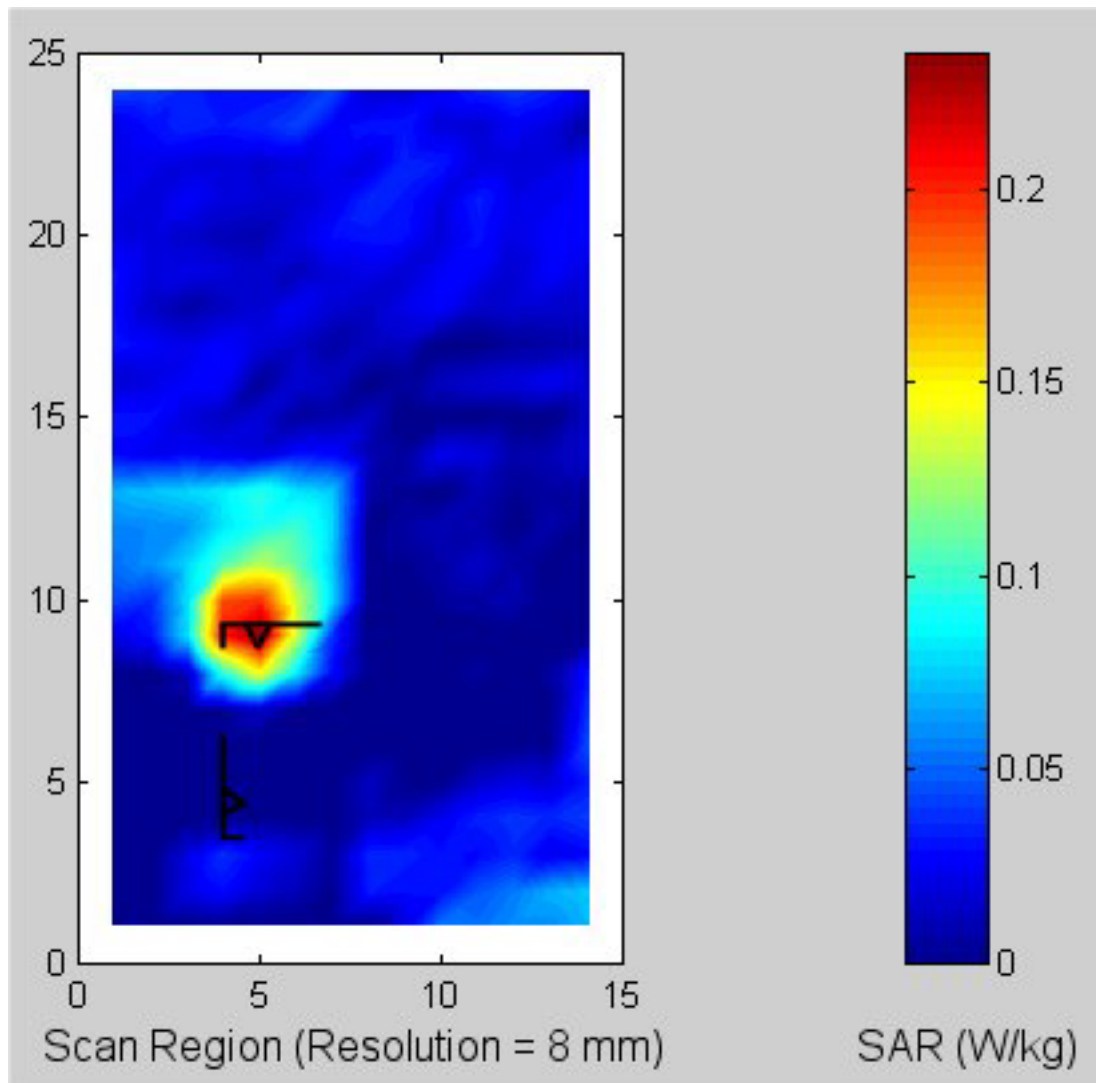


Fig. F.4. **Above-lap position (Configuration 1). Turbo mode at 5.25 GHz.** Coarse scan for the highest SAR region for the Senao Model NL-5354 CB Plus Aries2 Cardbus Adapter inserted into Dell Model PP01L Host Computer.

Table F.4. **Above-lap position (Configuration 1). Turbo mode at 5.25 GHz.** The SARs measured for the Senao Model NL-5354 CB Plus Aries2 Cardbus Adapter (FCC ID# NI3-AT53V214) inserted into Dell Model PP01L Host Computer.

1-g SAR = 0.244 W/kg

January 29, 2004

a. At depth of 1 mm

0.529	0.524	0.482	0.622	0.549
0.563	0.548	0.554	0.571	0.550
0.478	0.537	0.670	0.585	0.556
0.558	0.570	0.629	0.590	0.516
0.526	0.579	0.592	0.619	0.522

b. At depth of 3 mm

0.270	0.283	0.275	0.300	0.275
0.292	0.289	0.297	0.293	0.277
0.276	0.296	0.322	0.302	0.294
0.292	0.309	0.319	0.305	0.285
0.271	0.300	0.301	0.302	0.274

c. At depth of 5 mm

0.152	0.164	0.162	0.161	0.148
0.163	0.163	0.168	0.162	0.153
0.162	0.173	0.169	0.167	0.167
0.166	0.179	0.177	0.169	0.164
0.158	0.164	0.162	0.162	0.154

d. At depth of 7 mm

0.109	0.112	0.108	0.113	0.100
0.112	0.111	0.110	0.110	0.107
0.107	0.118	0.117	0.115	0.115
0.116	0.122	0.123	0.115	0.111
0.115	0.110	0.107	0.114	0.104

e. At depth of 9 mm

0.096	0.090	0.088	0.096	0.084
0.095	0.090	0.087	0.090	0.090
0.086	0.097	0.102	0.099	0.096
0.099	0.096	0.103	0.096	0.092
0.096	0.093	0.088	0.102	0.085

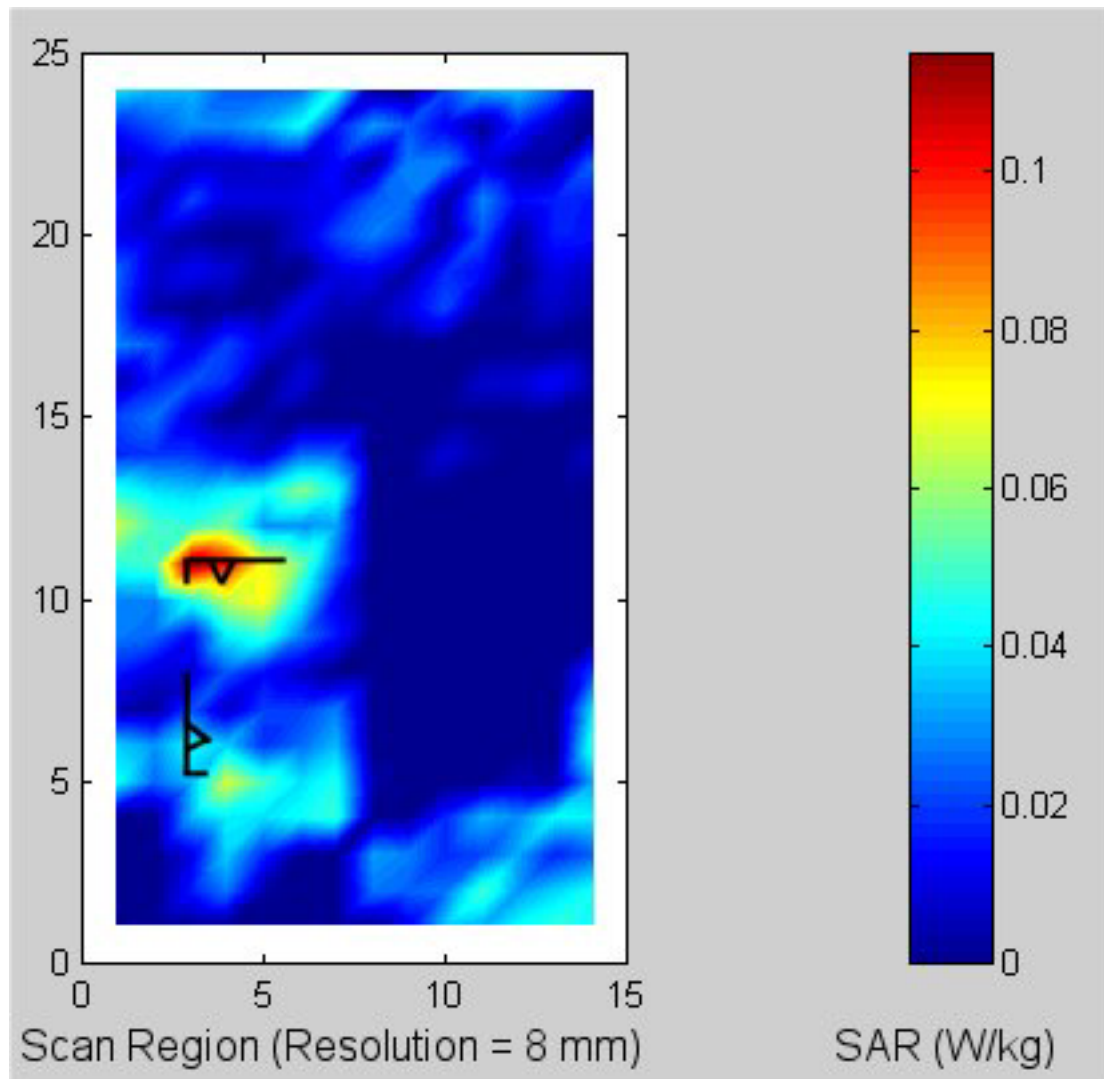


Fig. F.5. **Above-lap position (Configuration 1).** **Turbo mode at 5.29 GHz.** Coarse scan for the highest SAR region for the Senao Model NL-5354 CB Plus Aries2 Wireless Cardbus Adapter inserted into Dell Model PP01L Host Computer.

Table F.5. **Above-lap position (Configuration 1). Turbo mode at 5.29 GHz.** The SARs measured for the Senao Model NL-5354 CB Plus Aries2 Cardbus Adapter (FCC ID# NI3-AT53V214) inserted into Dell Model PP01L Host Computer.

1-g SAR = 0.116 W/kg

January 29, 2004

a. At depth of 1 mm

0.165	0.172	0.143	0.152	0.140
0.126	0.149	0.165	0.172	0.128
0.148	0.163	0.206	0.160	0.155
0.135	0.164	0.163	0.163	0.153
0.182	0.160	0.176	0.193	0.146

b. At depth of 3 mm

0.131	0.126	0.115	0.119	0.113
0.116	0.122	0.129	0.118	0.107
0.128	0.125	0.133	0.121	0.113
0.120	0.130	0.124	0.124	0.111
0.136	0.124	0.125	0.126	0.110

c. At depth of 5 mm

0.116	0.105	0.104	0.103	0.100
0.103	0.109	0.106	0.103	0.098
0.109	0.105	0.107	0.104	0.096
0.109	0.111	0.105	0.106	0.094
0.112	0.104	0.103	0.100	0.093

d. At depth of 7 mm

0.111	0.097	0.099	0.097	0.095
0.093	0.104	0.094	0.102	0.095
0.096	0.098	0.103	0.100	0.092
0.101	0.101	0.097	0.100	0.090
0.101	0.096	0.095	0.093	0.087

e. At depth of 9 mm

0.110	0.095	0.096	0.094	0.093
0.089	0.100	0.090	0.102	0.094
0.089	0.096	0.102	0.102	0.090
0.095	0.097	0.095	0.096	0.089
0.096	0.096	0.093	0.091	0.086

January 29, 2004

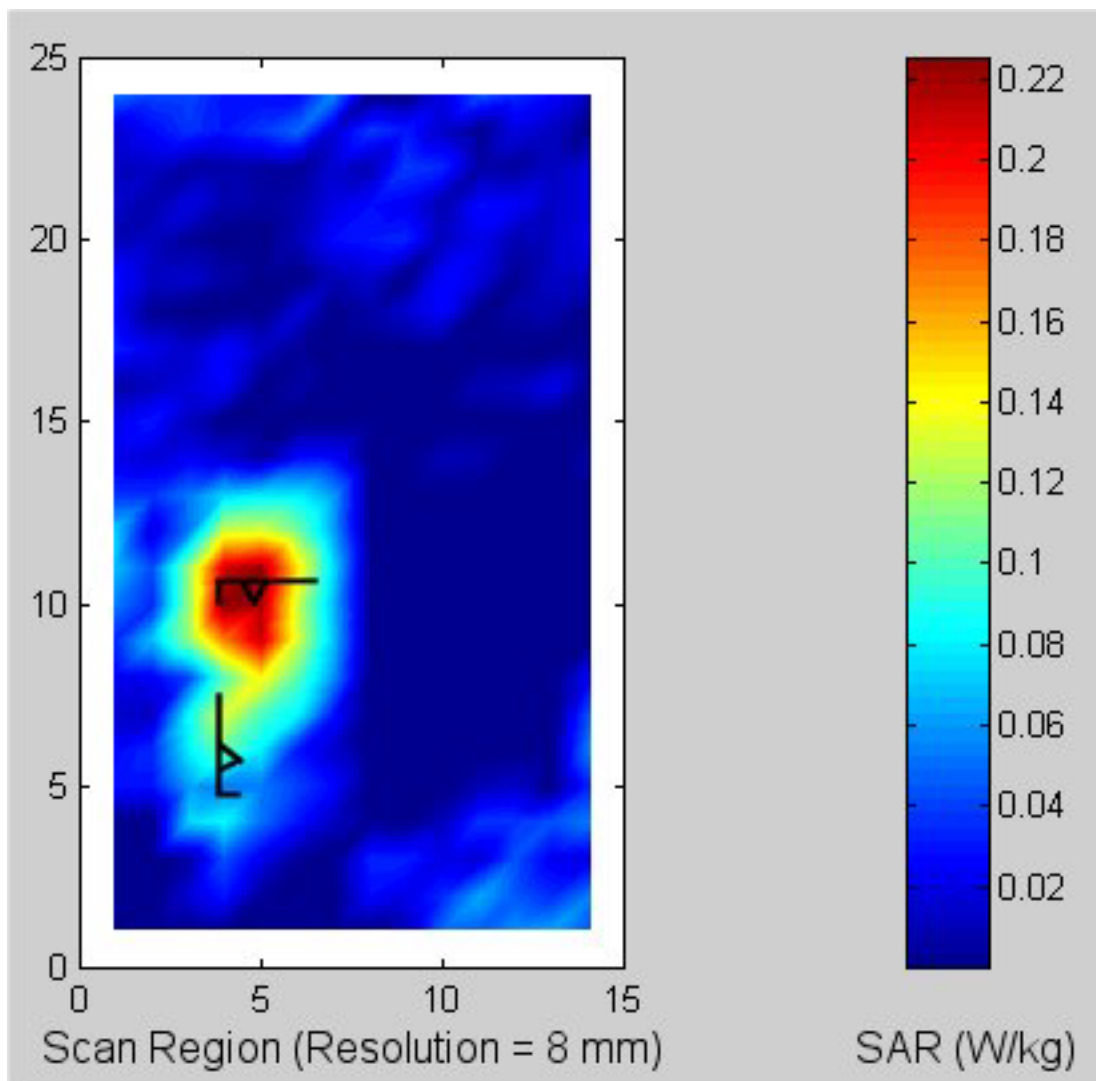


Fig. F.6. **Above-lap position (Configuration 1).** **Turbo mode at 5.80 GHz.** Coarse scan for the highest SAR region for the Senao Model NL-5354 CB Plus Aries2 Cardbus Adapter inserted into Dell Model PP01L Host Computer.

Table F.6. **Above-lap position (Configuration 1). Turbo mode at 5.80 GHz.** The SARs measured for the Senao Model NL-5354 CB Plus Aries2 Cardbus Adapter (FCC ID# NI3-AT53V214) inserted into Dell Model PP01L Host Computer.

1-g SAR = 0.236 W/kg

January 29, 2004

a. At depth of 1 mm

0.518	0.486	0.484	0.504	0.468
0.496	0.474	0.460	0.502	0.414
0.419	0.531	0.555	0.523	0.516
0.539	0.483	0.474	0.507	0.492
0.418	0.429	0.508	0.518	0.533

b. At depth of 3 mm

0.266	0.272	0.265	0.276	0.263
0.265	0.267	0.257	0.265	0.248
0.259	0.274	0.286	0.286	0.276
0.279	0.278	0.268	0.270	0.269
0.260	0.276	0.278	0.287	0.298

c. At depth of 5 mm

0.158	0.174	0.164	0.169	0.169
0.165	0.157	0.158	0.158	0.157
0.169	0.162	0.168	0.177	0.168
0.165	0.178	0.167	0.165	0.165
0.176	0.188	0.178	0.181	0.193

d. At depth of 7 mm

0.123	0.136	0.128	0.130	0.134
0.132	0.110	0.117	0.119	0.115
0.127	0.127	0.128	0.137	0.130
0.127	0.137	0.126	0.129	0.126
0.139	0.143	0.144	0.145	0.156

e. At depth of 9 mm

0.116	0.121	0.119	0.120	0.122
0.121	0.096	0.103	0.107	0.100
0.113	0.121	0.117	0.124	0.118
0.117	0.122	0.112	0.119	0.114
0.126	0.125	0.132	0.138	0.143

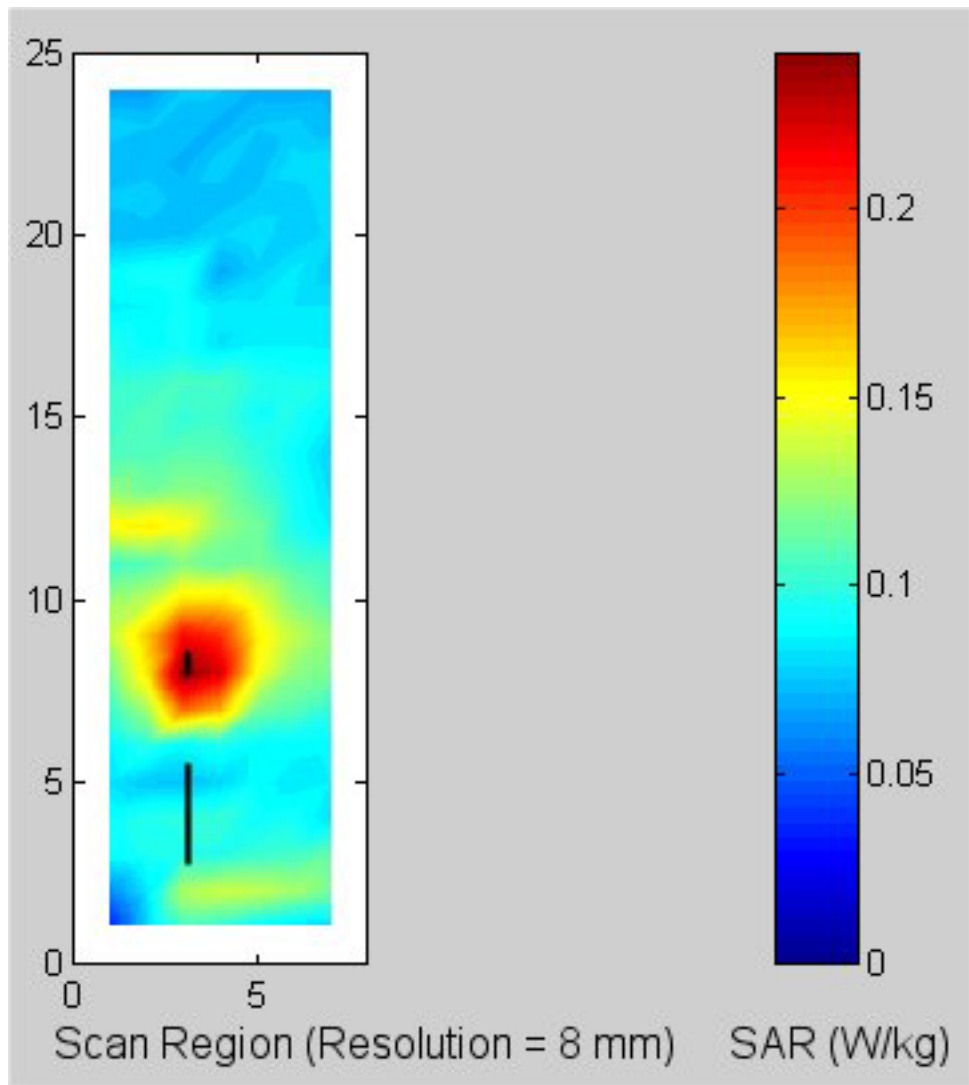


Fig. F.7. **Edge-on position (Configuration 2). Normal mode at 5.26 GHz.** Coarse scan for the highest SAR region for the Senao Model NL-5354 CB Plus Aries2 Cardbus Adapter inserted into Dell Model PP01L Host Computer.

Table F.7. **Edge-on position (Configuration 2). Normal mode at 5.26 GHz.** The SARs measured for the Senao Model NL-5354 CB Plus Aries2 Cardbus Adapter (FCC ID# NI3-AT53V214) inserted into Dell Model PP01L Host Computer.

1-g SAR = 0.213 W/kg

January 29, 2004

a. At depth of 1 mm

0.418	0.467	0.353	0.419	0.399
0.468	0.460	0.463	0.397	0.325
0.456	0.567	0.550	0.459	0.427
0.471	0.526	0.444	0.450	0.335
0.469	0.505	0.517	0.444	0.428

b. At depth of 3 mm

0.246	0.260	0.250	0.239	0.224
0.254	0.250	0.267	0.240	0.212
0.268	0.311	0.314	0.300	0.267
0.256	0.286	0.275	0.262	0.224
0.249	0.271	0.266	0.258	0.236

c. At depth of 5 mm

0.157	0.157	0.174	0.146	0.135
0.152	0.146	0.161	0.147	0.140
0.169	0.182	0.189	0.198	0.173
0.150	0.164	0.172	0.158	0.151
0.144	0.155	0.150	0.153	0.139

d. At depth of 7 mm

0.116	0.113	0.124	0.103	0.096
0.109	0.100	0.110	0.098	0.100
0.121	0.124	0.130	0.141	0.122
0.105	0.108	0.113	0.106	0.109
0.102	0.104	0.105	0.100	0.096

e. At depth of 9 mm

0.098	0.096	0.096	0.083	0.081
0.088	0.082	0.085	0.075	0.079
0.101	0.099	0.104	0.115	0.098
0.085	0.084	0.084	0.085	0.088
0.083	0.081	0.087	0.076	0.078

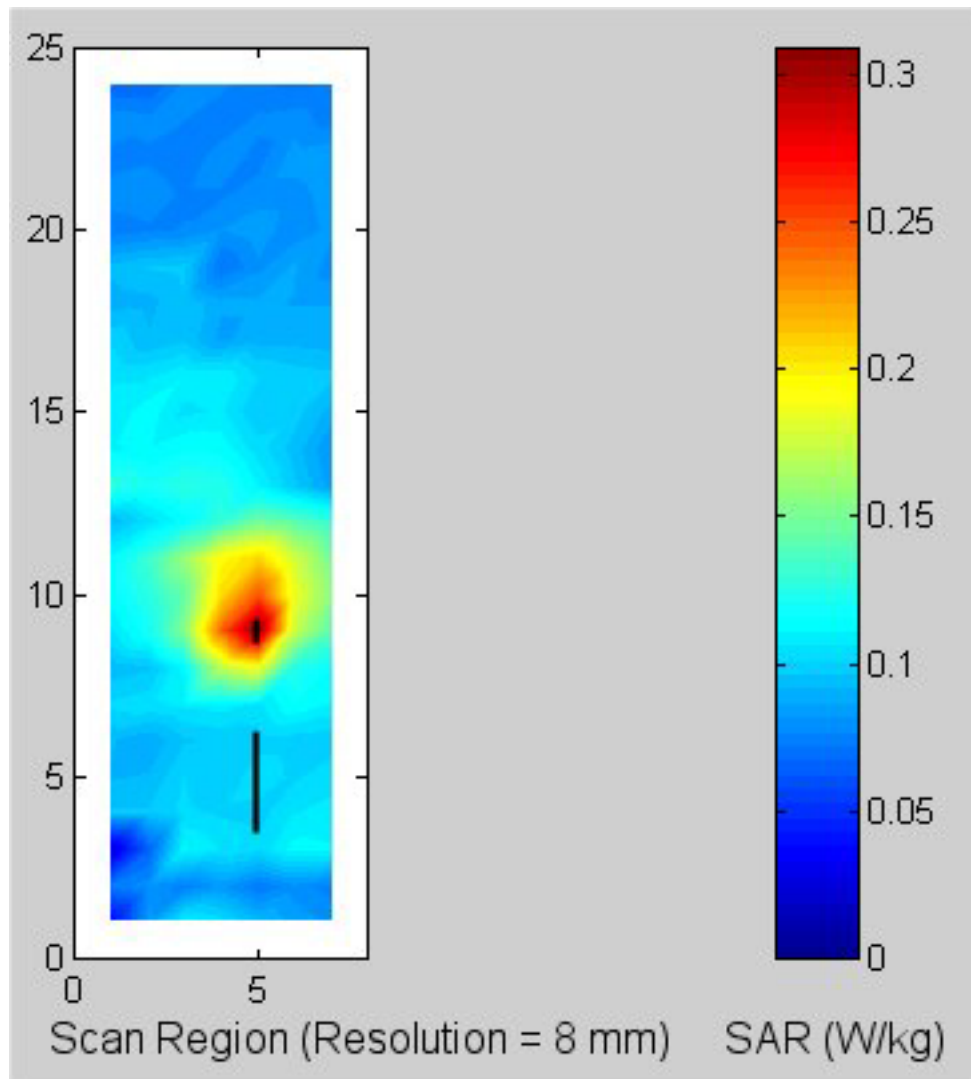


Fig. F.8. **Edge-on position (Configuration 2). Normal mode at 5.32 GHz.** Coarse scan for the highest SAR region for the Senao Model NL-5354 CB Plus Aries2 Cardbus Adapter inserted into Dell Model PP01L Host Computer.

Table F.8. **Edge-on position (Configuration 2). Normal mode at 5.32 GHz.** The SARs measured for the Senao Model NL-5354 CB Plus Aries2 Cardbus Adapter (FCC ID# NI3-AT53V214) inserted into Dell Model PP01L Host Computer.

1-g SAR = 0.265 W/kg

January 29, 2004

a. At depth of 1 mm

0.482	0.583	0.591	0.576	0.458
0.572	0.713	0.729	0.698	0.537
0.556	0.729	0.750	0.698	0.569
0.603	0.673	0.735	0.600	0.541
0.517	0.639	0.656	0.562	0.569

b. At depth of 3 mm

0.260	0.309	0.315	0.299	0.257
0.297	0.359	0.379	0.366	0.315
0.316	0.381	0.404	0.372	0.325
0.300	0.347	0.365	0.332	0.304
0.280	0.323	0.334	0.309	0.290

c. At depth of 5 mm

0.152	0.172	0.175	0.163	0.151
0.162	0.187	0.203	0.197	0.188
0.184	0.206	0.228	0.210	0.196
0.157	0.188	0.186	0.188	0.175
0.160	0.172	0.180	0.178	0.156

d. At depth of 7 mm

0.105	0.113	0.112	0.106	0.100
0.104	0.116	0.125	0.122	0.122
0.120	0.132	0.149	0.140	0.136
0.102	0.120	0.112	0.119	0.113
0.105	0.111	0.116	0.116	0.102

e. At depth of 9 mm

0.082	0.090	0.087	0.083	0.077
0.081	0.090	0.094	0.093	0.093
0.093	0.104	0.116	0.111	0.110
0.084	0.094	0.082	0.087	0.085
0.080	0.090	0.091	0.086	0.081

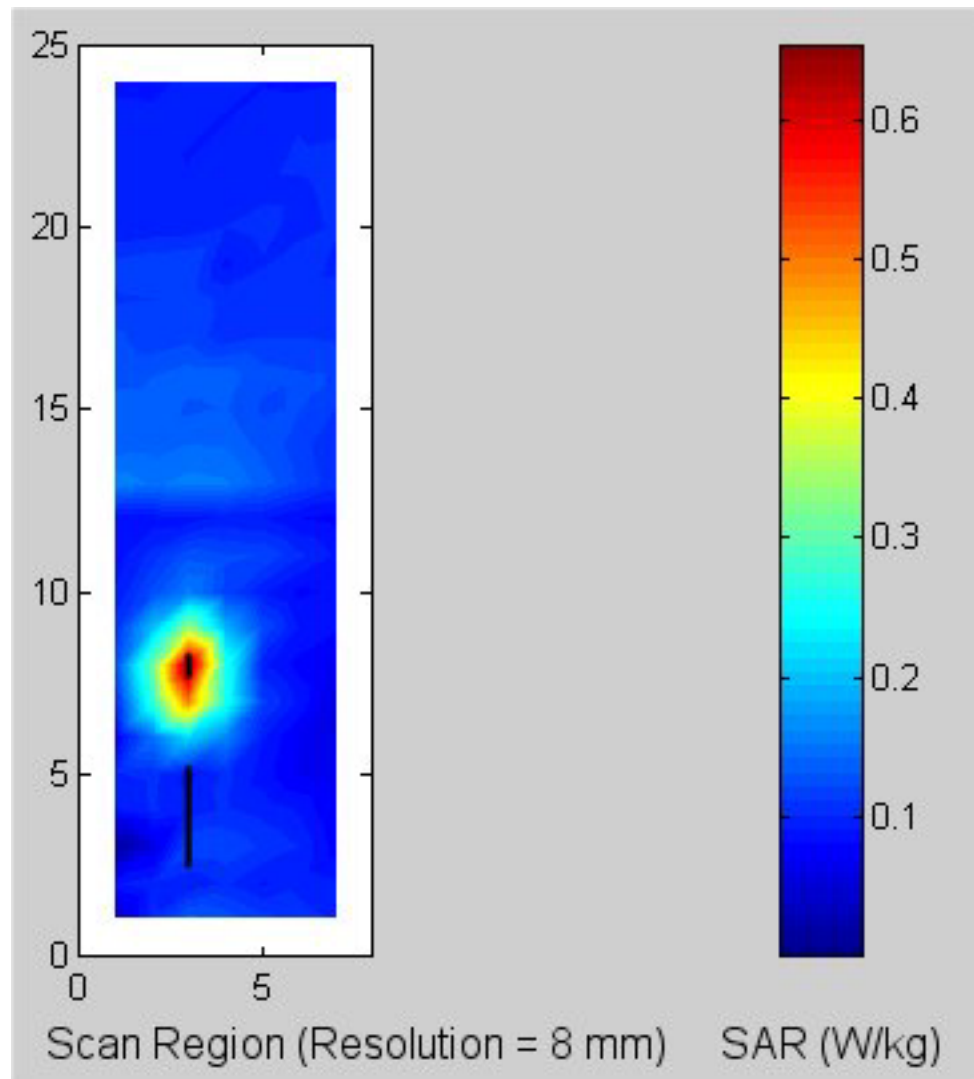


Fig. F.9. **Edge-on position (Configuration 2). Normal mode at 5.805 GHz.** Coarse scan for the highest SAR region for the Senao Model NL-5354 CB Plus Aries2 Cardbus Adapter inserted into Dell Model PP01L Host Computer.

Table F.9. **Edge-on position (Configuration 2). Normal mode at 5.805 GHz.** The SARs measured for the Senao Model NL-5354 CB Plus Aries2 Cardbus Adapter (FCC ID# NI3-AT53V214) inserted into Dell Model PP01L Host Computer.

1-g SAR = 0.638 W/kg

January 29, 2004

a. At depth of 1 mm

1.421	1.652	1.839	1.711	1.344
1.474	1.847	2.043	1.953	1.572
1.590	2.047	1.972	1.867	1.665
1.590	1.921	1.943	1.768	1.649
1.410	1.659	1.790	1.663	1.514

b. At depth of 3 mm

0.644	0.768	0.825	0.784	0.667
0.706	0.860	0.925	0.886	0.748
0.746	0.911	0.932	0.876	0.768
0.725	0.870	0.900	0.837	0.769
0.682	0.778	0.835	0.780	0.702

c. At depth of 5 mm

0.301	0.348	0.362	0.354	0.325
0.333	0.386	0.404	0.385	0.351
0.337	0.395	0.415	0.387	0.341
0.322	0.376	0.395	0.373	0.350
0.327	0.356	0.382	0.355	0.322

d. At depth of 7 mm

0.183	0.186	0.192	0.191	0.178
0.183	0.200	0.207	0.195	0.191
0.175	0.205	0.198	0.185	0.172
0.168	0.186	0.190	0.181	0.183
0.180	0.189	0.203	0.186	0.175

e. At depth of 9 mm

0.148	0.135	0.140	0.139	0.127
0.132	0.139	0.144	0.136	0.134
0.125	0.140	0.121	0.116	0.115
0.114	0.122	0.120	0.117	0.125
0.127	0.131	0.141	0.128	0.125

January 29, 2004

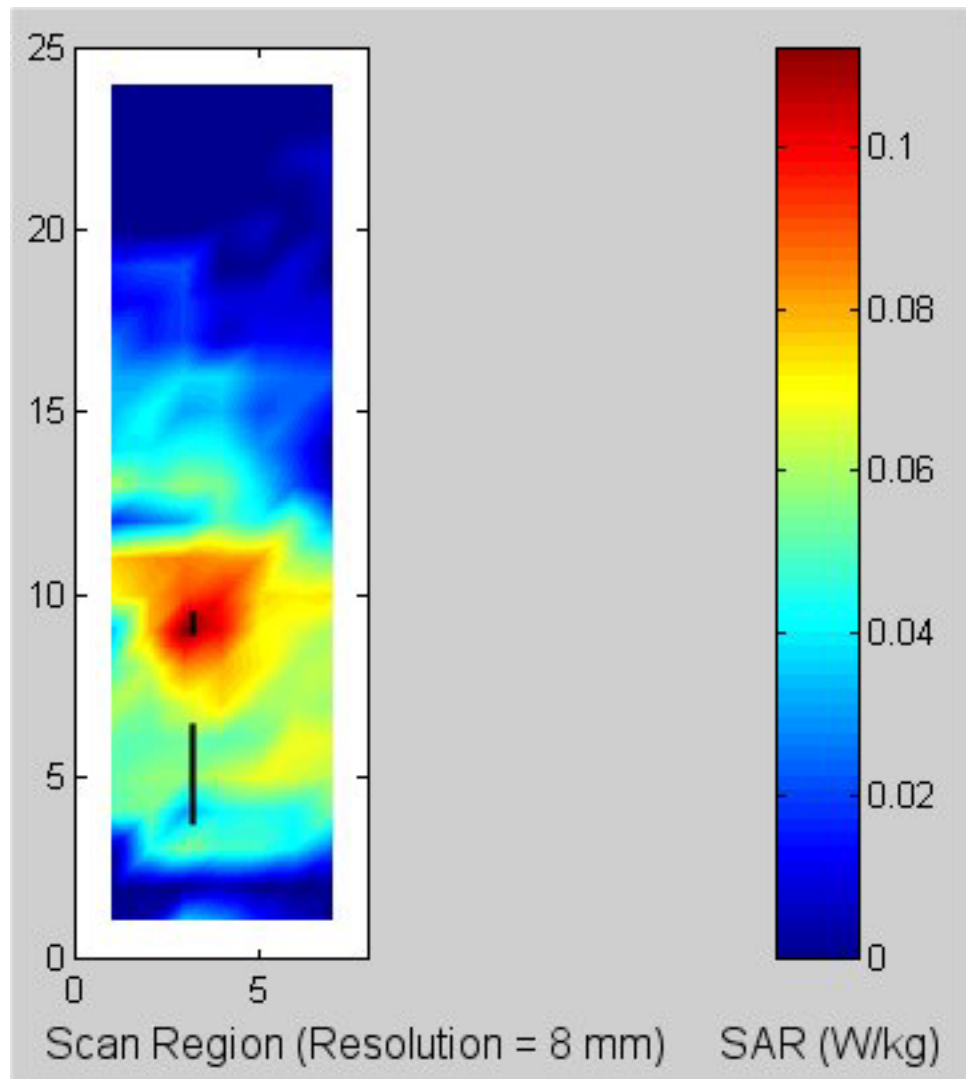


Fig. F.10. **Edge-on position (Configuration 2).** **Turbo mode at 5.25 GHz.** Coarse scan for the highest SAR region for the Senao Model NL-5354 CB Plus Aries2 Cardbus Adapter inserted into Dell Model PP01L Host Computer.

Table F.10. **Edge-on position (Configuration 2). Turbo mode at 5.25 GHz.** The SARs measured for the Senao Model NL-5354 CB Plus Aries2 Cardbus Adapter (FCC ID# NI3-AT53V214) inserted into Dell Model PP01L Host Computer.

1-g SAR = 0.113 W/kg

January 29, 2004

a. At depth of 1 mm

0.139	0.221	0.193	0.175	0.105
0.134	0.182	0.153	0.110	0.101
0.200	0.245	0.206	0.167	0.171
0.098	0.236	0.201	0.150	0.190
0.168	0.155	0.165	0.171	0.132

b. At depth of 3 mm

0.106	0.130	0.128	0.121	0.102
0.108	0.120	0.116	0.099	0.104
0.129	0.136	0.143	0.127	0.142
0.104	0.131	0.131	0.116	0.117
0.114	0.115	0.128	0.125	0.113

c. At depth of 5 mm

0.090	0.097	0.105	0.100	0.096
0.095	0.097	0.093	0.092	0.094
0.103	0.103	0.110	0.105	0.120
0.096	0.093	0.098	0.098	0.094
0.093	0.094	0.105	0.101	0.099

d. At depth of 7 mm

0.085	0.092	0.099	0.095	0.090
0.088	0.090	0.081	0.087	0.082
0.097	0.101	0.095	0.095	0.105
0.084	0.086	0.085	0.089	0.090
0.088	0.086	0.094	0.090	0.089

e. At depth of 9 mm

0.086	0.096	0.094	0.096	0.087
0.085	0.087	0.076	0.083	0.075
0.096	0.100	0.088	0.092	0.095
0.077	0.086	0.081	0.084	0.089
0.086	0.085	0.092	0.085	0.082

January 29, 2004

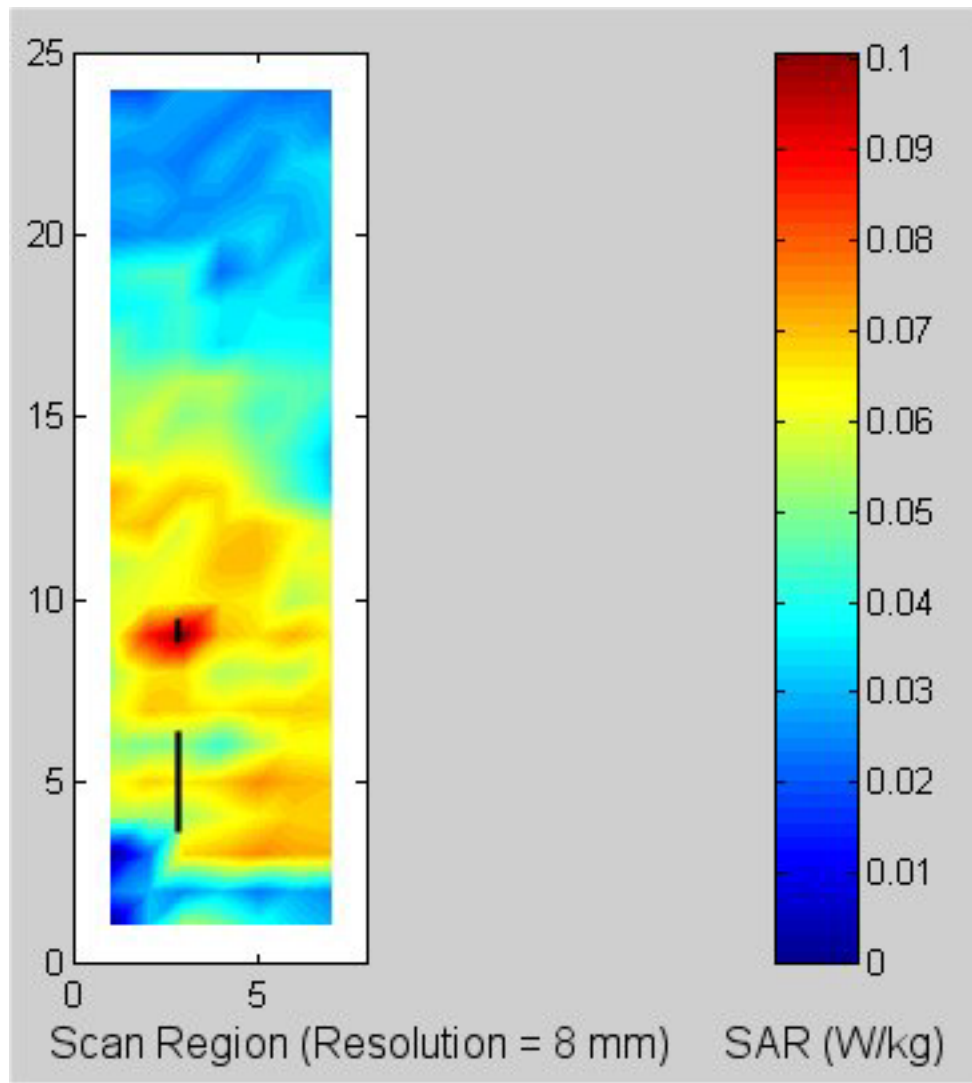


Fig. F.11. **Edge-on position (Configuration 2). Turbo mode at 5.29 GHz.** Coarse scan for the highest SAR region for the Senao Model NL-5354 CB Plus Aries2 Cardbus Adapter inserted into Dell Model PP01L Host Computer.

Table F.11. **Edge-on position (Configuration 2). Turbo mode at 5.29 GHz.** The SARs measured for the Senao Model NL-5354 CB Plus Aries2 Cardbus Adapter (FCC ID# NI3-AT53V214) inserted into Dell Model PP01L Host Computer.

1-g SAR = 0.105 W/kg

January 29, 2004

a. At depth of 1 mm

0.132	0.174	0.171	0.149	0.123
0.147	0.132	0.142	0.142	0.143
0.137	0.159	0.190	0.162	0.146
0.177	0.132	0.126	0.143	0.145
0.150	0.151	0.122	0.146	0.125

b. At depth of 3 mm

0.113	0.123	0.117	0.111	0.108
0.113	0.112	0.112	0.110	0.109
0.116	0.116	0.130	0.123	0.120
0.118	0.107	0.108	0.111	0.111
0.100	0.112	0.109	0.103	0.101

c. At depth of 5 mm

0.102	0.103	0.096	0.094	0.097
0.096	0.099	0.092	0.092	0.092
0.100	0.098	0.105	0.103	0.106
0.096	0.095	0.096	0.089	0.093
0.083	0.093	0.095	0.084	0.087

d. At depth of 7 mm

0.097	0.096	0.091	0.086	0.089
0.089	0.092	0.082	0.083	0.086
0.089	0.091	0.097	0.096	0.098
0.090	0.090	0.087	0.077	0.084
0.080	0.085	0.083	0.077	0.079

e. At depth of 9 mm

0.095	0.092	0.090	0.083	0.086
0.086	0.090	0.079	0.079	0.085
0.083	0.087	0.094	0.095	0.092
0.088	0.086	0.079	0.073	0.079
0.081	0.081	0.076	0.073	0.076

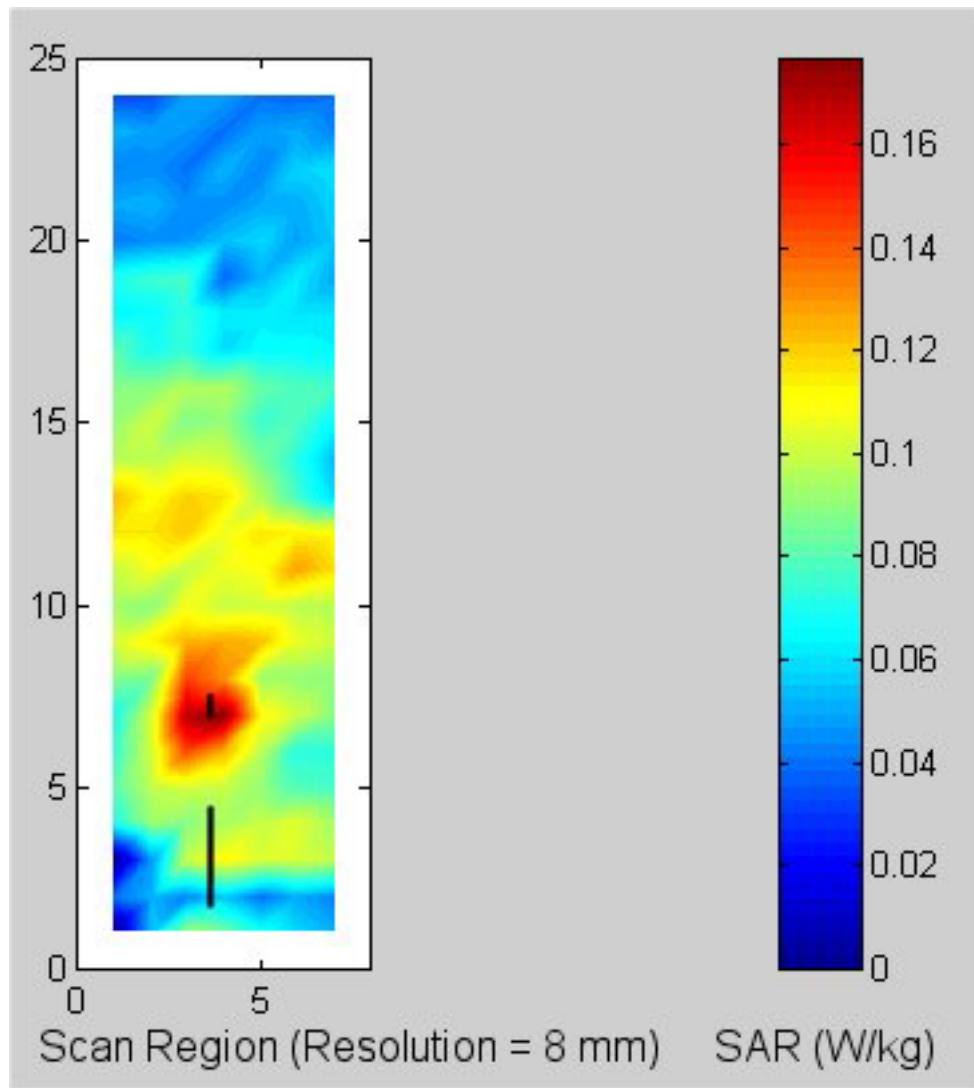


Fig. F.12. **Edge-on position (Configuration 2). Turbo mode at 5.80 GHz.** Coarse scan for the highest SAR region for the Senao Model NL-5354 CB Plus Aries2 Cardbus Adapter inserted into Dell Model PP01L Host Computer.

Table F.12. **Edge-on position (Configuration 2). Turbo mode at 5.80 GHz.** The SARs measured for the Senao Model NL-5354 CB Plus Aries2 Cardbus Adapter (FCC ID# NI3-AT53V214) inserted into Dell Model PP01L Host Computer.

1-g SAR = 0.180 W/kg

January 29, 2004

a. At depth of 1 mm

0.182	0.304	0.371	0.429	0.280
0.312	0.306	0.368	0.409	0.300
0.229	0.332	0.479	0.367	0.373
0.274	0.234	0.233	0.326	0.315
0.212	0.301	0.398	0.338	0.382

b. At depth of 3 mm

0.161	0.190	0.224	0.235	0.200
0.175	0.200	0.223	0.232	0.215
0.162	0.184	0.225	0.231	0.221
0.173	0.172	0.186	0.223	0.206
0.157	0.184	0.225	0.221	0.219

c. At depth of 5 mm

0.138	0.139	0.153	0.153	0.153
0.129	0.142	0.153	0.155	0.163
0.127	0.122	0.138	0.155	0.148
0.128	0.137	0.143	0.158	0.146
0.131	0.134	0.148	0.159	0.153

d. At depth of 7 mm

0.122	0.122	0.126	0.127	0.127
0.118	0.114	0.123	0.126	0.134
0.110	0.104	0.124	0.121	0.119
0.113	0.118	0.111	0.122	0.117
0.119	0.119	0.123	0.131	0.131

e. At depth of 9 mm

0.115	0.116	0.119	0.120	0.113
0.110	0.102	0.110	0.113	0.119
0.103	0.102	0.126	0.110	0.107
0.108	0.108	0.094	0.104	0.108
0.110	0.114	0.116	0.121	0.120

APPENDIX G

VARIATION OF SAR AS A FUNCTION OF DEPTH Z IN THE LIQUID FOR LOCATIONS OF THE HIGHEST SAR (FROM TABLES F.1 TO F.12)

January 29, 2004

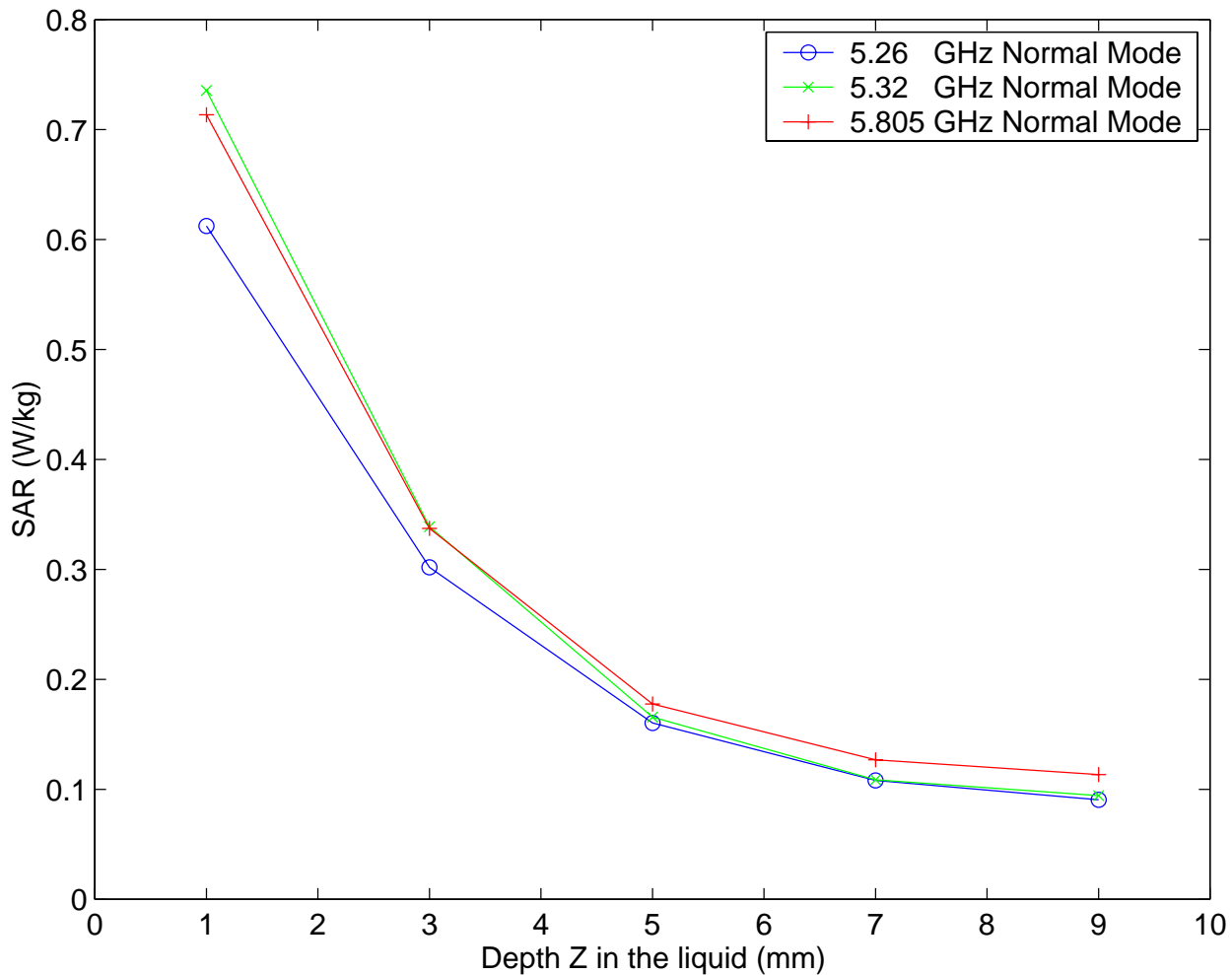


Fig. G.1. **Above-lap, Configuration 1.** Plot of the SAR variation as a function of depth Z in the liquid for locations of the highest SAR for the **normal** mode of Senao Model NL-5354 CB Plus Aries2 Cardbus Adapter inserted into Dell Model PP01L Host Computer (from Tables F.1 to F.3).

January 29, 2004

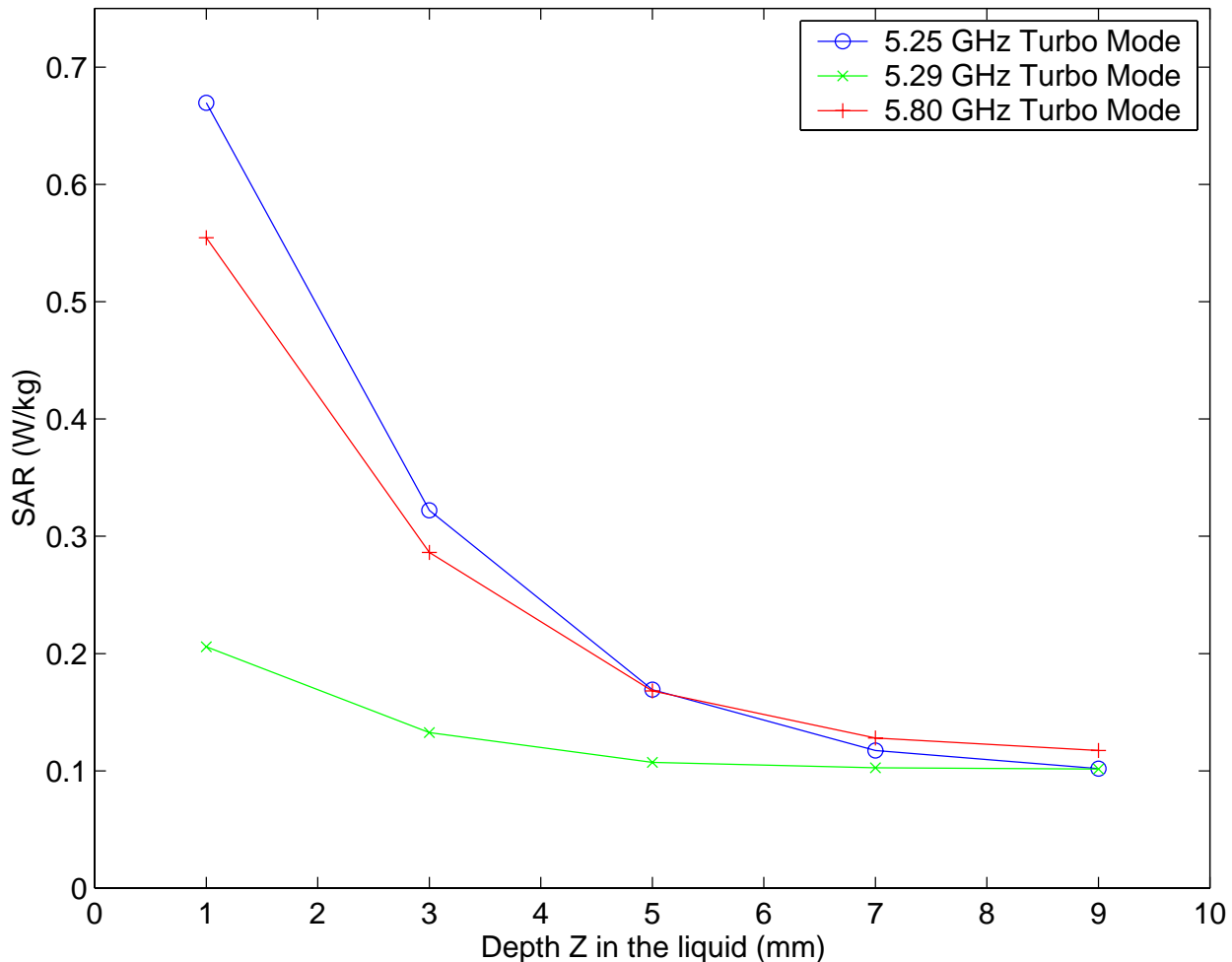


Fig. G.2. **Above-lap, Configuration 1.** Plot of the SAR variation as a function of depth Z in the liquid for locations of the highest SAR for the **turbo** mode of Senao Model NL-5354 CB Plus Aries2 Cardbus Adapter inserted into Dell Model PP01L Host Computer (from Tables F.4 to F.6).

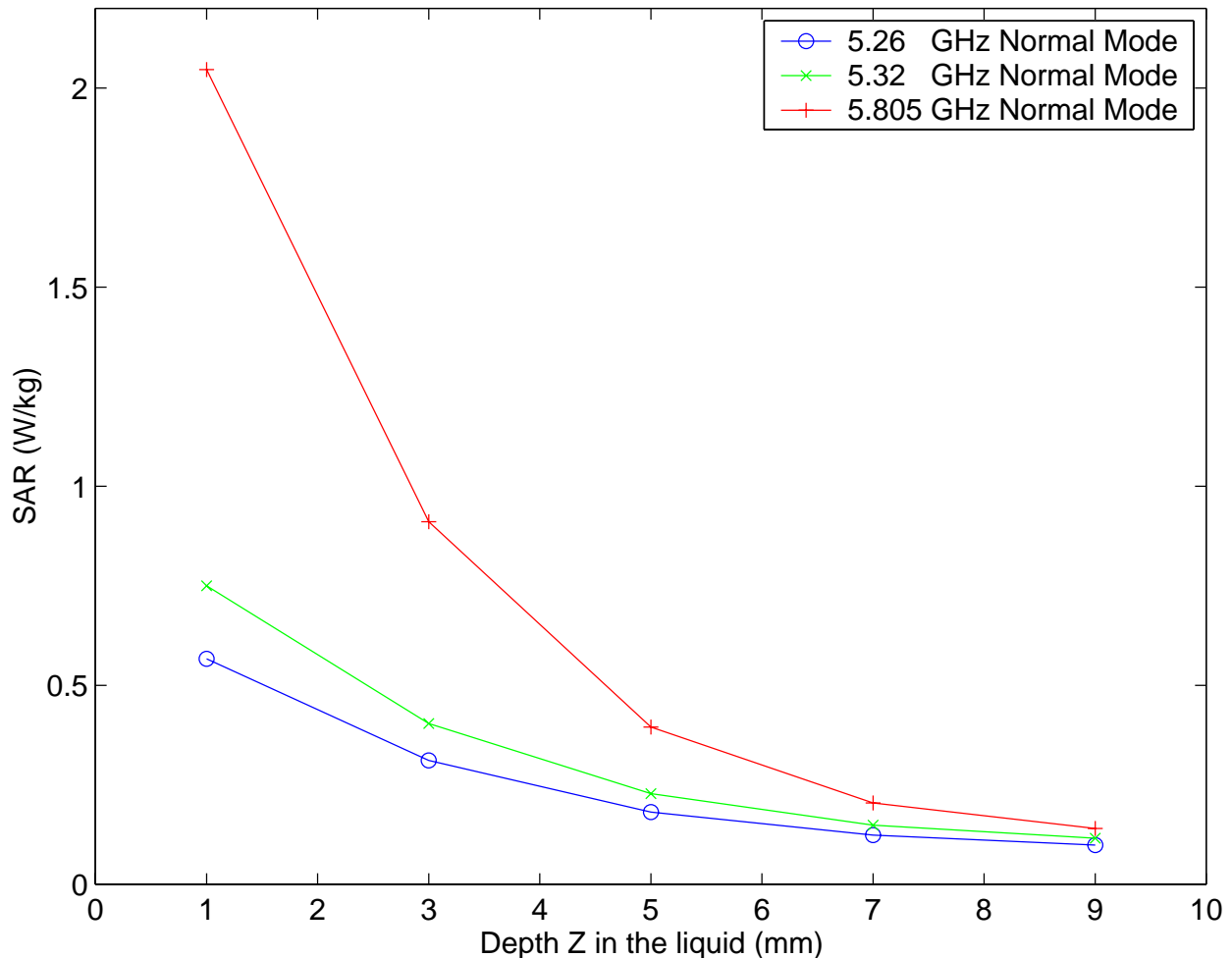


Fig. G.3. **Edge-on, Configuration 2.** Plot of the SAR variation as a function of depth Z in the liquid for locations of the highest SAR for the **normal** mode of Senao Model NL-5354 CB Plus Aries2 Cardbus Adapter inserted into Dell Model PP01L Host Computer (from Tables F.7 to F.9).

January 29, 2004

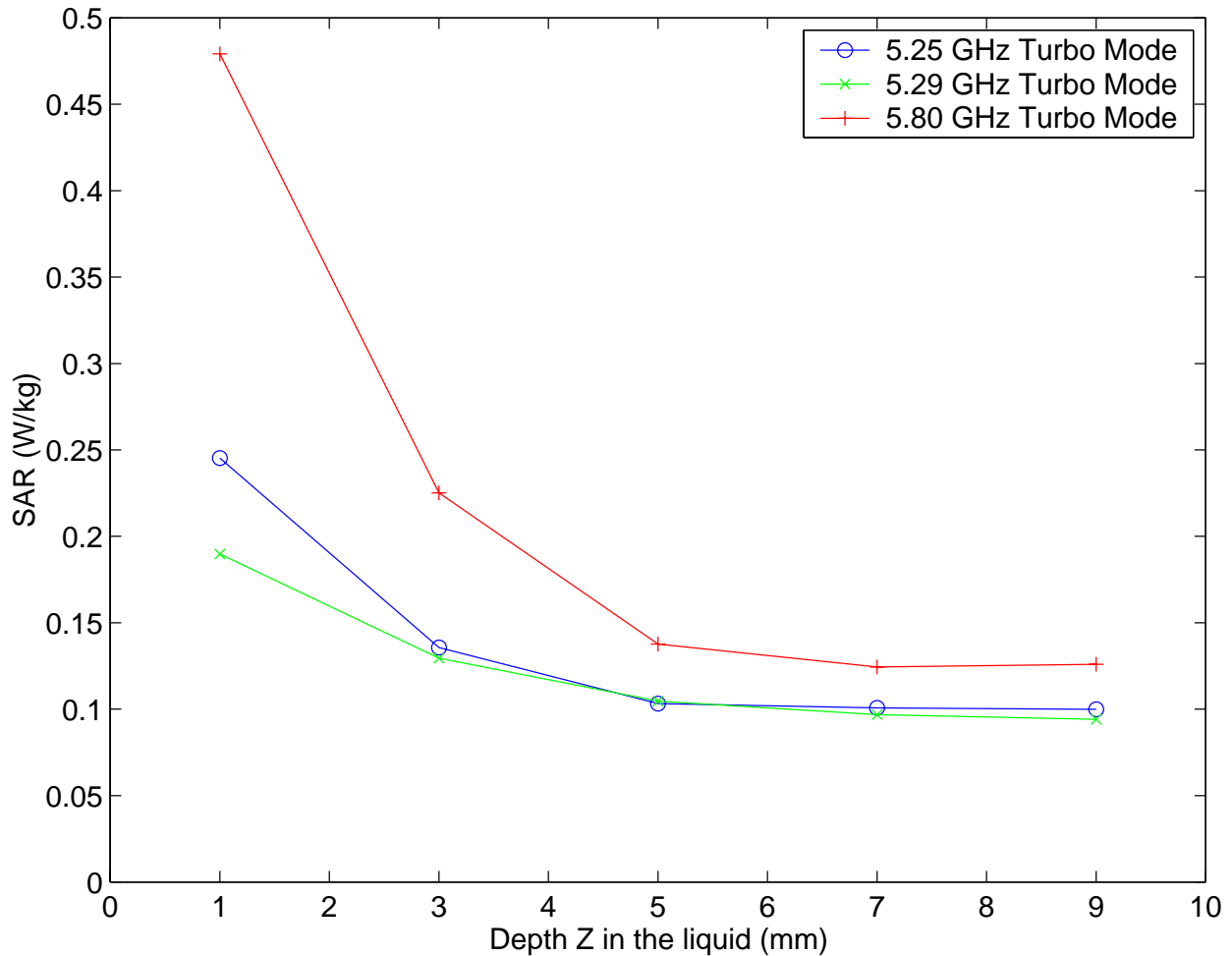


Fig. G.4. **Edge-on, Configuration 2.** Plot of the SAR variation as a function of depth Z in the liquid for locations of the highest SAR for the **turbo** mode of Senao Model NL-5354 CB Plus Aries2 Cardbus Adapter inserted into Dell Model PP01L Host Computer (from Tables F.10 to F.12).